

# Clearance and transport of amyloid $\beta$ by peripheral monocytes correlate with Alzheimer's disease progression

---

Received: 1 November 2023

---

Accepted: 2 September 2024

---

Published online: 12 September 2024

---

 Check for updates

---

Xin Huang<sup>1,2</sup>, Chris Fowler<sup>1</sup>, Yihan Li<sup>1</sup>, Qiao-Xin Li<sup>1,3</sup>, Jiaqi Sun<sup>1</sup>, Yijun Pan<sup>1</sup>, Liang Jin<sup>1</sup>, Keyla A. Perez<sup>1</sup>, Céline Dubois<sup>1</sup>, Yen Y. Lim<sup>4</sup>, Candace Drysdale<sup>1</sup>, Rebecca L. Rumble<sup>1</sup>, Holly R. Chinnery<sup>5,6,7</sup>, Christopher C. Rowe<sup>8</sup>, Ralph N. Martins<sup>9</sup>, Paul Maruff<sup>1,10</sup>, James D. Doecke<sup>11</sup>, Yong Lin<sup>12</sup>, Abdel A. Belaidi<sup>1</sup>, Kevin J. Barnham<sup>1</sup>, Colin L. Masters<sup>1</sup>✉ & Ben J. Gu<sup>1,2,12</sup>✉

Impaired clearance of amyloid  $\beta$  ( $A\beta$ ) in late-onset Alzheimer's disease (AD) affects disease progression. The role of peripheral monocytes in  $A\beta$  clearance from the central nervous system (CNS) is unclear. We use a flow cytometry assay to identify  $A\beta$ -binding monocytes in blood, validated by confocal microscopy, Western blotting, and mass spectrometry. Flow cytometry immunophenotyping and correlation with AD biomarkers are studied in 150 participants from the AIBL study. We also examine monocytes in human cerebrospinal fluid (CSF) and their migration in an APP/PS1 mouse model. The assay reveals macrophage-like  $A\beta$ -binding monocytes with high phagocytic potential in both the periphery and CNS. We find lower surface  $A\beta$  levels in mild cognitive impairment (MCI) and AD-dementia patients compared to cognitively unimpaired individuals. Monocyte infiltration from blood to CSF and migration from CNS to peripheral lymph nodes and blood are observed. Here we show that  $A\beta$ -binding monocytes may play a role in CNS  $A\beta$  clearance, suggesting their potential as a biomarker for AD diagnosis and monitoring.

Late-onset (sporadic) AD is a prevalent progressive neurodegenerative disorder. The onset of symptoms marks the beginning of the preclinical and prodromal stages, which span 20–30 years, followed by overt dementia<sup>1,2</sup>. During the preclinical stage, ~30% of CU elderly individuals exhibit increased retention of  $A\beta$ -PET ligands and reduced  $A\beta_{42}$  levels in CSF and plasma<sup>2</sup>.

The underlying pathogenic mechanisms of AD involve the failure of extracellular  $A\beta_{1-42}$  clearance and intraneuronal formation of tau-positive

tangles and neurites<sup>3-5</sup>.  $A\beta_{1-42}$  is produced from the proteolytic cleavage of amyloid precursor protein (APP), which is widely expressed in the CNS. The balance between  $A\beta_{1-42}$  production and clearance is critical for maintaining  $A\beta$  homeostasis in the brain. Microglial and astrocytic activation, along with pro-inflammatory responses, play key roles in clearing  $A\beta$  and interacting with tau and glial cells in the AD brain<sup>6,7</sup>.

Besides microglia clearing  $A\beta$  in the brain, Michaud et al. (2013) proposed a hypothesis on  $A\beta$  clearance by monocytes from the luminal

---

<sup>1</sup>The Florey Institute, The University of Melbourne, Parkville, VIC, Australia. <sup>2</sup>The Innate Phagocytosis Laboratory, Level 11, Melbourne, Victoria, Australia.

<sup>3</sup>National Dementia Diagnostics Laboratory, The University of Melbourne, Parkville, VIC, Australia. <sup>4</sup>Turner Institute for Brain and Mental Health, School of Psychological Sciences, Monash University, Clayton, VIC, Australia. <sup>5</sup>Optometry and Vision Sciences, The University of Melbourne, Parkville, Victoria, Australia. <sup>6</sup>Lions Eye Institute, Perth, Western Australia, Australia. <sup>7</sup>Optometry, School of Allied Health, The University of Western Australia, Perth, Australia.

<sup>8</sup>Department of Nuclear Medicine and Center for PET, Austin Health, Heidelberg, VIC, Australia. <sup>9</sup>Center of Excellence for Alzheimer's Disease Research and Care, Edith Cowan University, Joondalup, WA, Australia. <sup>10</sup>Cogstate Ltd., Melbourne, VIC, Australia. <sup>11</sup>Health and Biosecurity, Australian E-Health Research Center, CSIRO, Brisbane, QLD, Australia. <sup>12</sup>National Clinical Research Center for Aging and Medicine, Huashan Hospital, Fudan University, Shanghai, China.

✉ e-mail: [c.masters@unimelb.edu.au](mailto:c.masters@unimelb.edu.au); [ben.gu@innatephagolab.com.au](mailto:ben.gu@innatephagolab.com.au)

side of the brain vasculature<sup>8</sup>. Similarly, our previous human studies have shown a negative association between the innate phagocytic activity of peripheral monocytes and A $\beta$  accumulation in the brain, suggesting their potential involvement in A $\beta$  clearance in the CNS<sup>9</sup>. Sensitive, specific, and quantitative methods are needed to detect this phenomenon in the blood and to understand the underlying principles. Furthermore, animal experiments using mice models of AD have demonstrated that certain peripheral monocyte subsets can enter the brain<sup>10</sup>, which are defined as infiltrating monocytes. Given that monocytes often slip out of the bloodstream and settle in tissues, investigating whether these monocytes in CNS could overcome the blood-brain barrier (BBB) and travel back to the periphery is integral to understanding the A $\beta$  clearance pathways in AD pathogenesis.

This study aimed to understand how monocytes are involved in the communication between the peripheral blood and the CNS to clear A $\beta$  in AD. We explored the study in five sections: (1) We developed a flow cytometry-based assay to identify monocytes in the blood that strongly bind to A $\beta$ . This method was validated for sensitivity, specificity, and quantifiability using flow cytometry, confocal microscopy, Western blotting, and mass spectrum technologies; (2) We characterized the A $\beta$ -binding monocyte phenotypes and studied the A $\beta$  phagocytosis process to understand their function in A $\beta$  clearance; (3) We also explored the correlation between the abundance of these A $\beta$ -binding monocytes and established AD markers, such as brain A $\beta$  levels and cognitive decline, to assess their clinical association with AD; (4) In addition, we investigated the potential of peripheral monocytes to move into the brain by examining their presence in CSF, shedding light on their activity within the CNS; and (5) Finally, animal experiments demonstrated the migration of these monocytes from the CNS to the periphery, illustrating their role in clearing A $\beta$  and providing insights into their potential as therapeutic targets. This structured approach aimed to advance our understanding of the involvement of peripheral monocytes in A $\beta$  clearance and their implications for AD diagnosis and treatment.

## Results

### A flow cytometry-based assay that accurately identified A $\beta$ -binding monocytes in the blood

**Comparative analysis of anti-A $\beta$  monoclonal antibodies.** We assessed several anti-human A $\beta$  monoclonal antibodies for their ability to identify A $\beta$ -binding monocytes in six blood samples (3 CU, 2 MCI, and 1 AD-Dementia) using flow cytometry. The antibodies included clones W0-2<sup>11</sup>, 4G8, and 6E10, with 22C11, an anti-APP mAb, serving as a control. Our results showed that most monocytes in the blood did not carry A $\beta$ , with only a very small number showing A $\beta$  binding. Among the antibodies tested, W0-2 demonstrated the highest sensitivity, followed by 4G8 and 6E10; In contrast, 22C11 was unable to recognize A $\beta$  on the surface of monocytes (Supplementary Fig. 1). This difference in recognition ability may be due to variations in the antigenic sites targeted by the different antibodies. A diagram illustrating the binding domains of the antibodies used in this study is presented in Supplementary Fig. 2.

In addition, typical flow cytometry histograms provided a clear visual representation of fluorescence intensity of the secondary antibody (expressed as % of Max), which is proportional to the level of A $\beta$  on cell surfaces after A $\beta$  peptide binding by human blood leukocytes (Supplementary Fig. 3) and monocyte subsets (Fig. 1a). Cells within the green circles exhibited substantial binding of A $\beta$  peptides, confirming the presence of A $\beta$  peptides on the cell surface of monocytes.

To verify our findings, human peripheral blood mononuclear cells (5 PBMCs, all CU) were stained with W0-2 and 6E10 mAbs to detect surface ( $n=3$ ) and intracellular A $\beta$  ( $n=2$ ), respectively. Further examination using Z-stack imaging revealed the co-localization of surface and intracellular A $\beta$  peptides in intermediate monocytes (Fig. 1b). This confirmed the existence of A $\beta$ -binding monocytes in the

blood, particularly intermediate monocytes carrying A $\beta$  peptides on their cell surface and inside the cytoplasm.

**Validation of the assay and confirmation of the affinity of CD14<sup>+</sup>CD16<sup>+</sup> monocytes to synthetic A $\beta$ <sub>1-42</sub> peptides.** Following the identification of the A $\beta$ -binding monocytes using the flow cytometry-based W02 mAb and secondary antibody assay in blood samples, validating this assay was crucial. This validation involved incubating human blood ( $n=6$ , all CU) with synthetic A $\beta$ <sub>1-42</sub> peptides to confirm the specificity of the assay (Fig. 2a).

Our results demonstrated a significant binding of A $\beta$ <sub>1-42</sub> peptides to human monocytes compared to the DMSO vehicle control (Tukey's multiple comparisons test  $q=11.74$ , DF = 30, adjusted  $p<0.0001$ ; Fig. 2b). Importantly, this binding remained intact even after the wash procedure, indicating a strong affinity. In contrast, lymphocytes and neutrophils did not exhibit comparable levels of binding to A $\beta$ <sub>1-42</sub> peptides, as shown by one-way ordinary ANOVA ( $F(5, 30)=33.38$ ,  $P<0.0001$ ) and subsequent Tukey's multiple comparisons tests (monocytes vs. lymphocytes  $q=13.69$ , DF = 30, adjusted  $p<0.0001$ ; monocytes vs. neutrophils  $q=14.08$ , DF = 30, adjusted  $p<0.0001$ , Fig. 2b). These analyses confirmed the binding capacity of periphery monocytes to A $\beta$ <sub>1-42</sub> peptides in the blood, which was not observed among lymphocytes and neutrophils.

Furthermore, the three subsets of monocytes demonstrated different A $\beta$ <sub>1-42</sub> binding capacities. Intermediate (CD14<sup>+</sup>CD16<sup>+</sup>) monocytes exhibited the highest binding capacity to synthetic A $\beta$ <sub>1-42</sub> peptides compared with the vehicle control (Tukey's multiple comparisons test  $q=11.86$ , DF = 30, adjusted  $p<0.0001$ ), which was significantly higher than that of non-classical (CD14<sup>+</sup>CD16<sup>-</sup>) monocytes (Tukey's multiple comparisons test  $q=5.378$ , DF = 30, adjusted  $p=0.0033$ ; Fig. 2c). Classical (CD14<sup>+</sup>CD16<sup>-</sup>) monocytes displayed the lowest binding capacity. Significant differences were observed among the three subsets, as determined by one-way ordinary ANOVA ( $F(5, 30)=32.13$ ,  $P<0.0001$ ) and Tukey's multiple comparisons tests (intermediate vs. non-classical  $q=8.689$ , DF = 30, adjusted  $p<0.0001$ ; intermediate vs. classical  $q=14.07$ , DF = 30, adjusted  $p<0.0001$ ; non-classical vs. classical  $q=5.378$ , DF = 30, adjusted  $p=0.0078$ , Fig. 2c).

Taken together, our application of the A $\beta$ <sub>1-42</sub> binding assay using human blood pre-incubated with synthetic A $\beta$ <sub>1-42</sub> peptides validated the specific binding of monocytes to A $\beta$ <sub>1-42</sub> peptides, particularly among intermediate CD14<sup>+</sup>CD16<sup>+</sup> monocytes. This supported the authenticity of identifying A $\beta$ -binding monocytes in blood samples, mirroring the in vivo scenario.

### Confirmation of the presence of A $\beta$ <sub>1-42</sub> on A $\beta$ -binding monocytes in the blood.

Additional validation tests were crucial to verify the presence of A $\beta$ <sub>1-42</sub> peptides on these monocytes, considering their potential role in clearing A $\beta$  from the brain. PBMCs from four CU individuals were sorted based on CCR2 and CD14 expression. CCR2 was selected as a surrogate marker for cell sorting because of its use in priming with the anti-A $\beta$  antibody W0-2 for Western blotting and mass spectrometry analyses. The resulting CCR2<sup>+</sup>CD14<sup>+</sup>, CCR2<sup>+</sup>CD14<sup>-</sup>, and CCR2<sup>-</sup>CD14<sup>-</sup> populations were examined using multiple techniques. Western blots, employing W0-2 mAb for priming, showed substantial amounts of A $\beta$ <sub>1-42</sub> peptides on CCR2<sup>+</sup>CD14<sup>+</sup> monocytes, but smaller amounts on CCR2<sup>-</sup>CD14<sup>+</sup> monocytes, while no signal of A $\beta$ <sub>1-42</sub> peptides was detected on CCR2<sup>-</sup>CD14<sup>-</sup> lymphocytes (Fig. 3a). Two distinct A $\beta$  bands emerged: a 9–14 KD band representing A $\beta$ <sub>1-42</sub> dimer/tetramer, and a 4.5 KD band indicating A $\beta$ <sub>1-42</sub> monomer. Over 90% of A $\beta$ <sub>1-42</sub> peptides on CCR2<sup>+</sup>CD14<sup>+</sup> monocytes were shown in the dimer/tetramer form, while CCR2<sup>-</sup>CD14<sup>+</sup> monocytes demonstrated a balanced mix of oligomers and monomers.

The results were further corroborated through SELDI-TOF mass spectrometry, where the sorted PBMCs from two CU individuals were immune-precipitated by W0-2 mAb. Diverse A $\beta$ <sub>1-42</sub> species, including

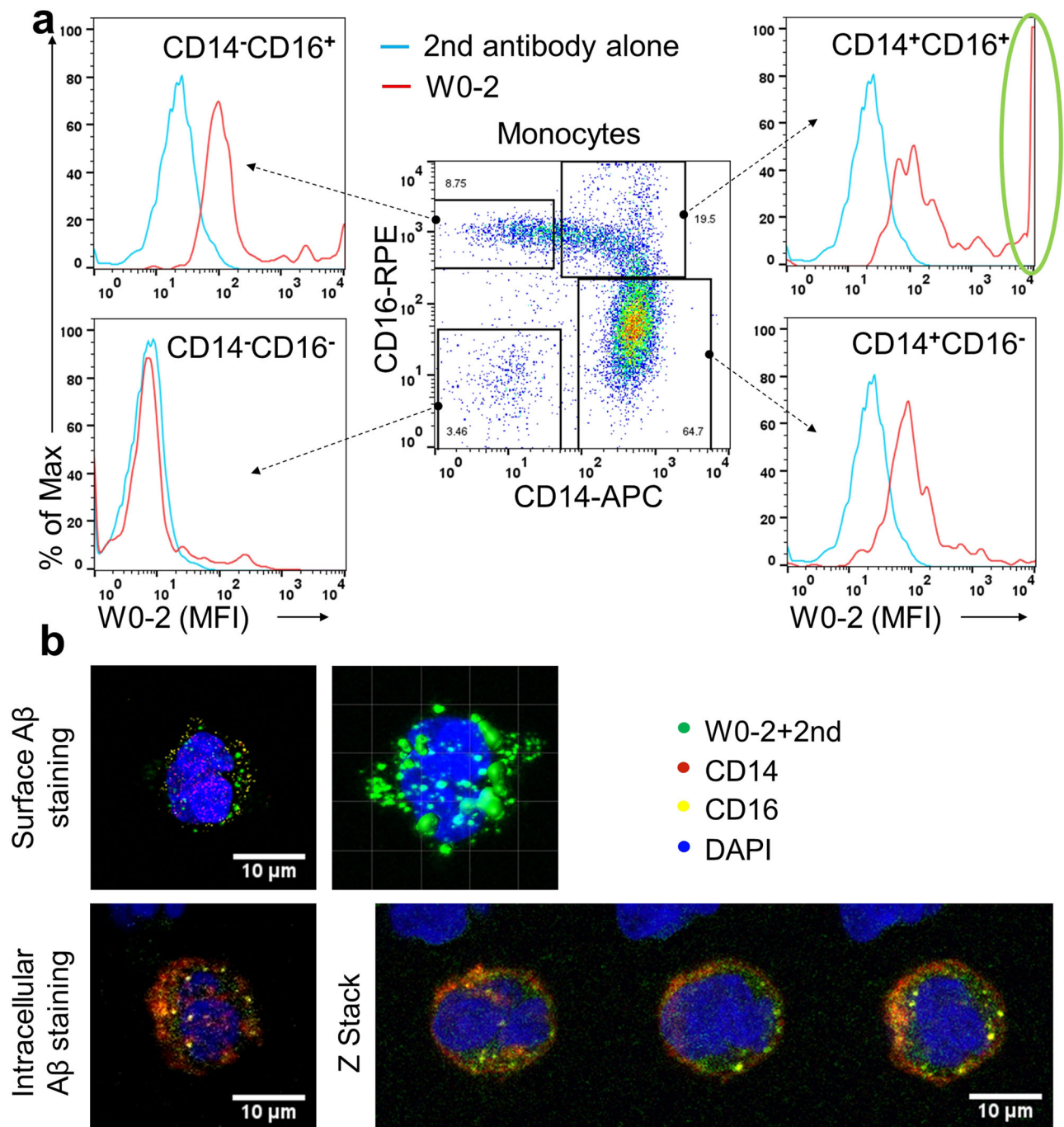


**Fig. 1 | The flow cytometry-based assay.** **a** Flow cytometry dot plot outlined monocyte subsets based on CD14 and CD16 expression, displaying surface A $\beta$  detection on monocytes via W0-2 and secondary antibodies in the histograms. **b** Confocal microscopy displayed A $\beta$  peptides on the surface and cytoplasm of

intermediate monocytes, identified by CD14 and CD16 ( $n = 3$ ). Intracellular A $\beta$  was observed using the 6E10 mAb and captured through Z-stack imaging ( $n = 2$ ). Nuclei were counter-stained with DAPI. MFI: The mean fluorescence intensity.

dimers, were detected in CCR2<sup>+</sup>CD14<sup>+</sup> and CCR2<sup>+</sup>CD14<sup>-</sup> monocytes, while CCR2<sup>-</sup>CD14<sup>-</sup> lymphocytes exhibited no presence of A $\beta$ <sub>1-42</sub> (Fig. 3b). Moreover, triple-quadrupole mass spectrometry (TQ-MS) identified the fragments of 28-42 (A $\beta$ -specific) on various cell types from three CU individuals, which included CCR2<sup>+</sup>CD14<sup>+</sup> and CCR2<sup>+</sup>CD14<sup>-</sup> monocytes, and CCR2<sup>-</sup>CD14<sup>-</sup> lymphocytes. Fragment 16-27 (sourced from A $\beta$  and APP) was also detected in abundance (Fig. 3c). Together, Western blotting and mass spectrometry confirmed the presence of A $\beta$ <sub>1-42</sub> peptides on the surface of A $\beta$ -binding monocytes.

### Characterization of A $\beta$ -binding monocytes

**Peripheral A $\beta$ -binding monocytes exhibit a macrophage-like phenotype associated with A $\beta$  phagocytosis function.** We used four-color immunophenotypic analysis to characterize the phenotypes of the A $\beta$ -binding monocytes. The characterization relied on basic monocyte classification using CD14 and CD16 antibodies, with additional phenotypic markers introduced into the flow cytometry assay either individually or as a pair ( $n \geq 3$ , with a total of 22 blood samples analyzed, regardless of clinical classification).

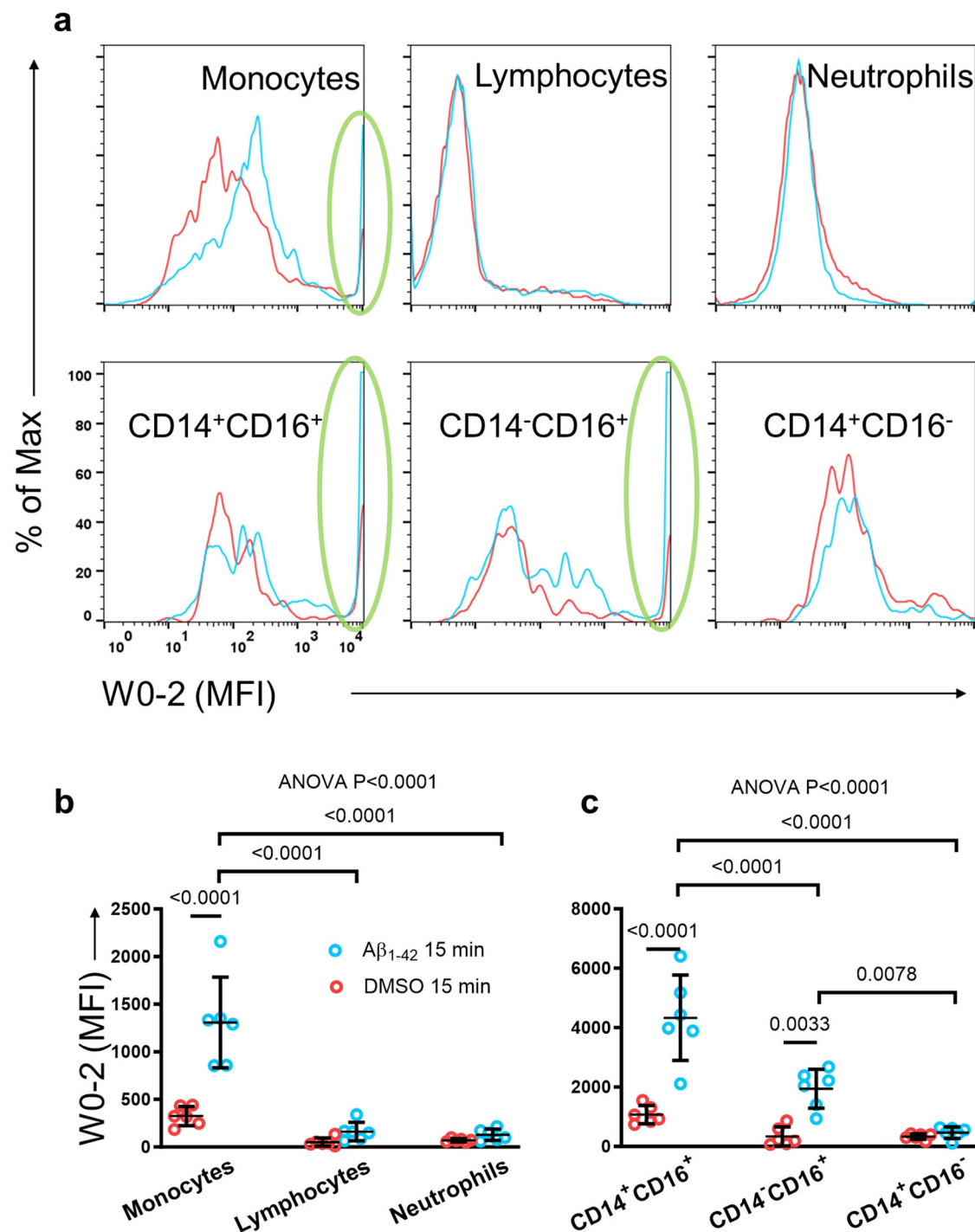


**Fig. 2 | The affinity of monocytes to synthetic Aβ<sub>1-42</sub> peptides.** Human blood samples ( $n = 6$ , all CU) were incubated with synthetic Aβ<sub>1-42</sub> peptides to validate the assay's specificity. **a** Monocytes showed significant binding compared to the DMSO (circled). Lymphocytes and neutrophils did not show comparable binding. Among monocyte subsets, CD14<sup>+</sup>CD16<sup>+</sup> and CD14<sup>-</sup>CD16<sup>+</sup> monocytes exhibited significant Aβ<sub>1-42</sub> binding (circled). CD14<sup>+</sup>CD16<sup>-</sup> monocytes did not show binding. **b, c** These

findings confirm the specific binding of monocytes to Aβ<sub>1-42</sub> peptides, particularly CD14<sup>+</sup>CD16<sup>+</sup> and CD14<sup>-</sup>CD16<sup>+</sup> monocytes. The column dot plots represent mean ± standard deviation. All datasets were normally distributed. Group comparison was determined by one-way ordinary ANOVA, followed by Tukey's multiple comparisons test (solid zig-zag line).

Results showed that these Aβ-binding monocytes were LIN-1<sup>+</sup> and HLA-DR<sup>+</sup> (i.e., MHC-II), indicating their differentiation from dendritic cells (Fig. 4a, b). These cells also expressed chemotactic receptors CX3CR1 and CCR2, indicating strong migratory capabilities (Fig. 4c, d). In addition, they exhibited CD68<sup>+</sup> macrophage-like and TREM2<sup>+</sup> microglia-like phenotypes (Fig. 4e, f). In contrast, the remaining CD14<sup>+</sup>CD16<sup>+</sup> monocytes lacked expressions of these two markers.

Notably, CD68<sup>+</sup> monocytes accounted for  $0.05 \pm 0.03\%$  of total monocytes, and TREM2<sup>+</sup> monocytes accounted for  $0.06 \pm 0.06\%$  of total monocytes ( $n = 6$ , regardless of clinical classification). Furthermore, Aβ-binding monocytes expressed various Aβ-binding receptors<sup>12,13</sup>, including CD85A/LILRB3, CD85D/LILRB2 receptors (Fig. 4g, h), and CD91/LRP1 (Fig. 4i). These cells also expressed complement receptors (CD11b, CD11c, and CD35/CR1) (Fig. 4j-l), and

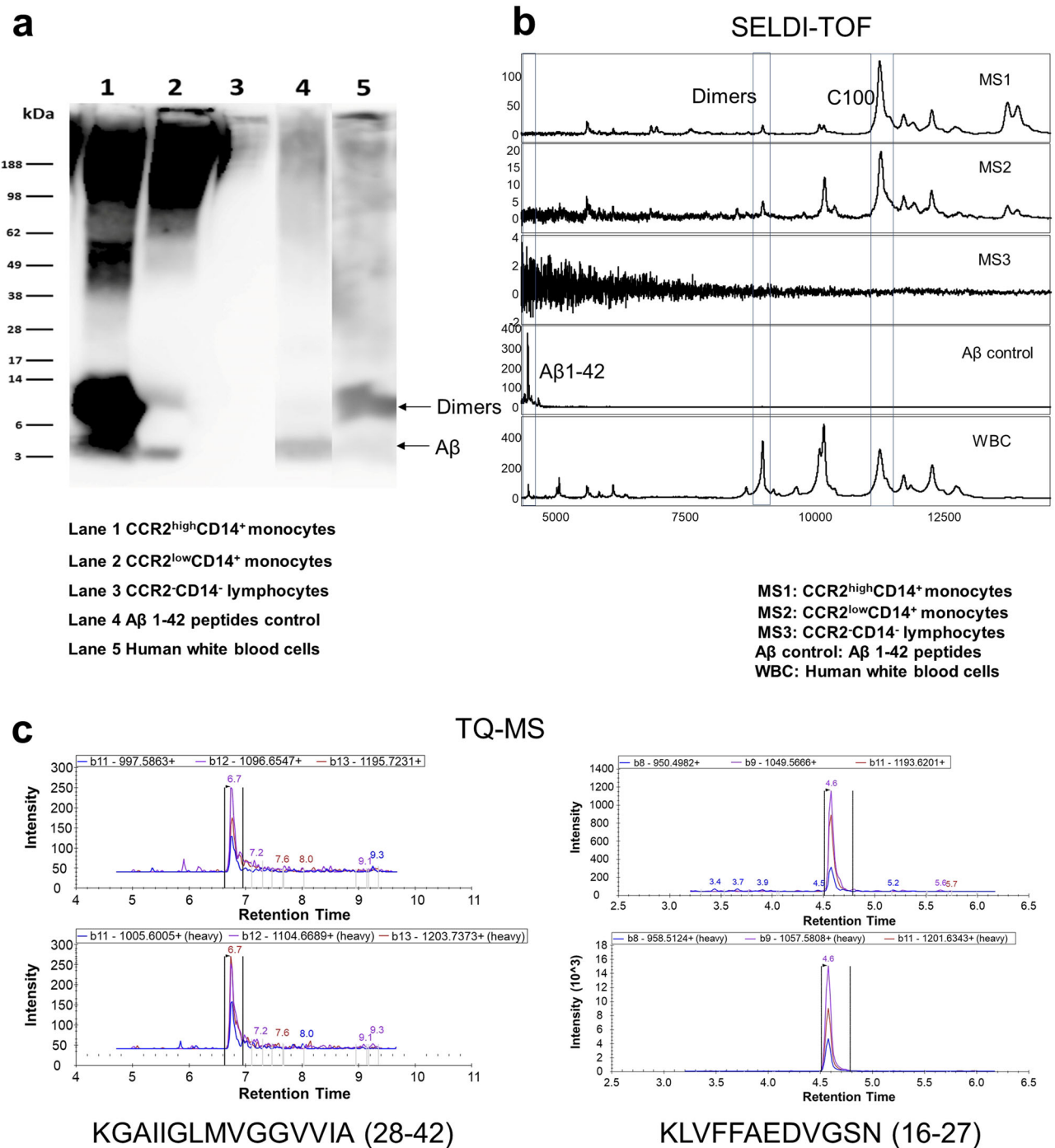


**Fig. 3 | Confirmation of Aβ<sub>1-42</sub> presence on Aβ-binding monocytes in blood.** PBMCs from CU individuals were FACS sorted based on CCR2 and CD14 expression. **a** Western blots ( $n = 2$ ) showed substantial Aβ<sub>1-42</sub> on CCR2<sup>+</sup>CD14<sup>+</sup> monocytes, smaller amounts on CCR2<sup>low</sup>CD14<sup>+</sup> monocytes, and no signal on CCR2<sup>-</sup>CD14<sup>-</sup> lymphocytes. **b** SELDI-TOF mass spectrometry ( $n = 2$ ) confirmed diverse Aβ<sub>1-42</sub> species,

including dimers, in CCR2<sup>+</sup>CD14<sup>+</sup> and CCR2<sup>low</sup>CD14<sup>+</sup> monocytes, but not in CCR2<sup>-</sup>CD14<sup>-</sup> lymphocytes. **c** TQ-MS ( $n = 3$ ) identified Aβ-specific fragments (28–42) on various cell types, including CCR2<sup>+</sup>CD14<sup>+</sup> and CCR2<sup>low</sup>CD14<sup>+</sup> monocytes, and CCR2<sup>-</sup>CD14<sup>-</sup> lymphocytes, with fragment (16–27) also detected abundantly.

receptors associated with phagocytosis function (MerTK, P2X7R, CD163 and CD33) (Fig. 4m–p). Notably, Aβ<sup>+</sup> monocytes displayed elevated expression levels for CCR2 ( $n = 7$ , Aβ<sup>+</sup> vs. Aβ<sup>-</sup> monocytes:  $66.7 \pm 37.8$  vs.  $24.3 \pm 6.2$  (Mean  $\pm$  SD), Wilcoxon matched-pairs signed rank test  $P = 0.047$  with two-tails), CD68 ( $n = 7$ ,  $974.7 \pm 886.5$  vs.  $5.5 \pm 1.1$ , Wilcoxon matched-pairs signed rank test  $P = 0.016$ ), and TREM2 ( $n = 6$ ,  $166.8 \pm 253.1$  vs.  $6 \pm 1.6$ , Wilcoxon matched-pairs signed rank test  $P = 0.063$ ), compared to Aβ<sup>-</sup> monocytes (asterisk in Fig. 2d–f).

Subsequently, we examined monocyte subsets. Across intermediate (CD14<sup>+</sup>CD16<sup>+</sup>), non-classical (CD14<sup>-</sup>CD16<sup>+</sup>), and classical (CD14<sup>+</sup>CD16<sup>-</sup>) monocyte subsets, the Aβ-binding monocytes exhibited similar immune phenotyping characteristics (Supplementary Fig. 4).

#### Phagocytic activity of monocytes correlating with surface Aβ levels

To investigate the association between surface Aβ levels on monocytes and their phagocytic functions, we took another cohort of three

## Monocytes

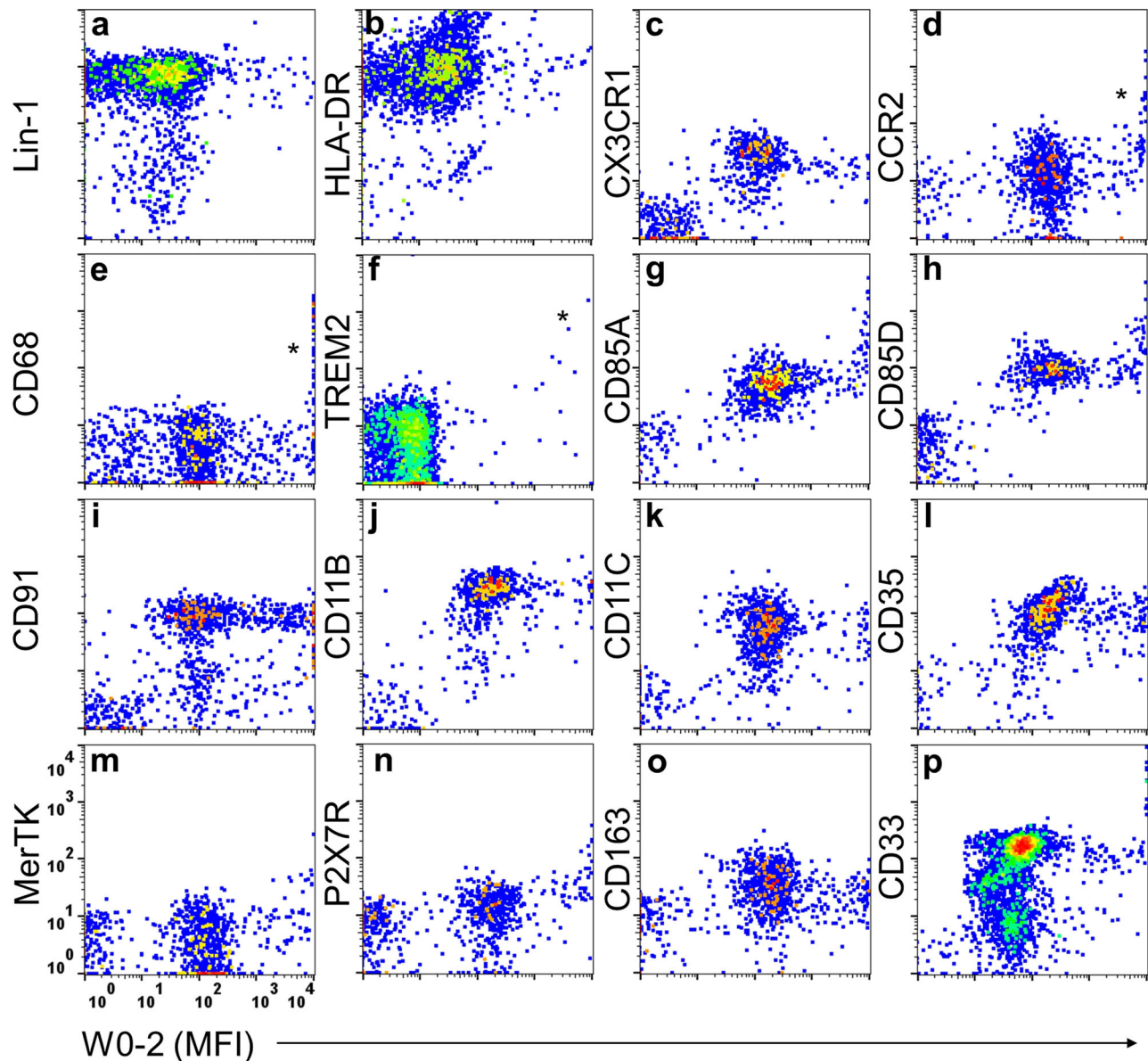


**Fig. 4 | Characterization of A $\beta$ -binding monocytes.** Peripheral A $\beta$ -binding monocytes ( $n \geq 3$ , with a total of 22 blood samples analyzed) were analyzed using four-color immunophenotypic analysis. A $\beta$ -binding monocytes exhibited a LIN-1<sup>+</sup> and HLA-DR<sup>+</sup> (MHC-II) phenotype (a, b), indicating differentiation from dendritic cells, and expressed CX3CR1 and CCR2 chemotactic receptors (c, d), suggesting strong migratory capabilities. They also showed CD68<sup>+</sup> macrophage-like (e) and

TREM2<sup>+</sup> microglia-like phenotypes (f). A $\beta$ -binding monocytes expressed A $\beta$ -binding receptors (CD85A, CD85D, CD91) (g–i), complement receptors (CD11b, CD11c, CD35) (j–l), and phagocytosis-associated receptors (MerTK, P2X7R, CD163, CD33) (m–p). It is worth noting that in the four-color panel for TREM2 (f), what matches TREM2, CD14, and CD16 was Qdot525 conjugated W0-2, unlike in the other panels where W0-2 was used in conjunction with a secondary antibody.

individuals (1 CU, 1 MCI, and 1 AD-dementia) and separated their PBMCs. The CD14<sup>+</sup> monocytes were categorized arbitrarily into A $\beta$ <sup>-</sup>, A $\beta$ <sup>+</sup>, and A $\beta$ <sup>++</sup> monocytes based on their surface A $\beta$  levels (Supplementary Fig. 5). The uptake of yellow-orange (YO) beads by these three monocyte populations was assessed using a well-established, real-time tri-color flow cytometry phagocytosis function assay<sup>9</sup>. The area under curves (AUC) of YO beads by A $\beta$ <sup>++</sup>, A $\beta$ <sup>+</sup>, and A $\beta$ <sup>-</sup> monocytes were  $219392 \pm 20589$ ,  $184012 \pm 27627$ , and  $109437 \pm 11056$  (arbitrary unit), respectively, indicating their different phagocytic abilities. The results showed that CD14<sup>+</sup>A $\beta$ <sup>++</sup> monocytes exhibited the highest phagocytic activity, followed by CD14<sup>+</sup>A $\beta$ <sup>+</sup> monocytes, while CD14<sup>+</sup>A $\beta$ <sup>-</sup> monocytes displayed the lowest uptake of YO beads (Friedman test  $P = 0.0278$ ,

followed by Dunn's multiple comparisons test: CD14<sup>+</sup>A $\beta$ <sup>++</sup> vs. CD14<sup>+</sup>A $\beta$ <sup>-</sup> monocytes adjusted  $P = 0.0429$ ).

#### A $\beta$ phagocytosis: tracing the journey from extracellular to intracellular

To investigate monocyte phagocytic activity, we developed a Two-Color Fluorescent Reporting System to monitor monocyte/microglial phagocytosis of oligomerized A $\beta$ <sub>1-42</sub> (oA $\beta$ <sub>1-42</sub>) in real-time. This system incorporated AF647-conjugated Aducanumab to visualize surface-bound oA $\beta$ <sub>1-42</sub> and pHrodo red to highlight intra-lysosomal oA $\beta$ <sub>1-42</sub>. We employed flow cytometry at multiple time points (0.5, 1, 2, 4, and 24 h) for continuous observation.

**Table 1 | Demographics of the AIBL study cohort**

Demographics	Control ( $\leq 25\text{CL}$ ) <sup>a</sup>	Case ( $> 25\text{CL}$ )
Number of Participants (n)	66	84
Age (mean (SD))	74.85 (7.46)	75.31 (7.42)
Sex = Male (%)	27 (40.9)	46 (54.8)
Years of Education (mean (SD))	12.91 (3.11)	12.40 (2.98)
<b>APOE genotype (%)</b>		
E2/E2	1 (1.5)	0 (0.0)
E2/E3	10 (15.2)	0 (0.0)
E2/E4	3 (4.5)	2 (2.4)
E3/E3	37 (56.1)	28 (33.3)
E3/E4	14 (21.2)	38 (45.2)
E4/E4	1 (1.5)	16 (19.0)
<b>Clinical Classification (%)</b>		
AD-dementia	8 (12.1)	28 (33.3)
CU	49 (74.2)	29 (34.5)
MCI	9 (13.6)	27 (32.1)
Image PET Centiloid (mean (SD))	2.74 (11.73)	89.15 (32.44)
MMSE (mean (SD))	28.05 (2.38)	25.27 (5.09)
CDR (mean (SD))	0.28 (0.70)	0.58 (0.61)
Episodic Memory (mean (SD))	0.28 (0.90)	-0.50 (1.46)
Composite PACC score (mean (SD))	0.25 (0.79)	-1.07 (2.00)

<sup>a</sup>Stratified by brain A $\beta$ -PET burden.

The demographic table was used for binary logistic regression, leading to the reclassification of the study cohort into two groups:  $\leq 25$  CL and  $> 25$  CL, rather than using categories such as AD-dementia, MCI, and CU.

Initially, we focused on pHrodo-oA $\beta_{1-42}$  phagocytosis by various cell types, including neuronal (HT22), glial (U251) cells, and microglial cells (BV2). BV2 cells exhibited surface adhesion of pHrodo-oA $\beta_{1-42}$  followed by internalization after 2 h, while most peptides were phagocytosed into lysosomes by 24 h (Supplementary Fig. 6). After 2 h, HT22 cells displayed surface adhesion without subsequent internalization, while U251 cells exhibited surface adhesion with weak internalization. In both cell types, internalization became more apparent after 24 h (Supplementary Fig. 7).

We then studied the phagocytic function of human PBMCs. Preliminary results suggest that peripheral monocytes from three individuals (1 CU, 1 MCI, and 1 AD-dementia) all showed substantial internalization of pHrodo-oA $\beta_{1-42}$  after 24 h (Suppl. Fig. 8). Notably, classic monocytes (CD14<sup>+</sup>CD16<sup>-</sup>) differentiated into intermediate monocytes (CD14<sup>+</sup>CD16<sup>+</sup>) after a 24-h treatment with pHrodo-oA $\beta_{1-42}$ , resulting in an increased percentage of intermediate monocytes over the total of intermediate and classic monocytes [= intermediate/(intermediate + classic)  $\times$  100%] -- from  $6.6 \pm 2.7$  at 2 h to  $63.3 \pm 23.8$  at 24 h, suggesting a pro-inflammatory response upon pHrodo-oA $\beta_{1-42}$  treatment (Supplementary Fig. 8).

### Peripheral monocyte surface A $\beta$ quantification: a potential biomarker for AD

**An overview.** Quantifying A $\beta$  on the surface of peripheral monocytes could serve as a potential biomarker for AD, providing a non-invasive method for early detection and monitoring. Our study involved 150 participants, including 78 CU, 36 MCI, and 36 AD-dementia individuals. The cohort consisted of 73 males and 77 females, with a mean age of 75 years.

In addition, based on A $\beta$ -PET burden (Centiloid, CL) in the brain, 84 individuals in the cohort had A $\beta$ -PET burden more than 25 CL, indicating higher brain A $\beta$  deposition, while 66 individuals had A $\beta$ -PET

**Table 2 | An overview of flow cytometry results**

Tube of WO-2+2nd	CU (n = 78)	MCI (n = 36)	AD-Dementia (n = 36)
% of Lymphocytes	24.4 $\pm$ 6.8	23.9 $\pm$ 6.7	26 $\pm$ 9.7
% of Monocytes	6.1 $\pm$ 2.2	6.2 $\pm$ 2	6.2 $\pm$ 2.4
% of A $\beta^{++}$ Monocytes	1.3 $\pm$ 1.1	0.7 $\pm$ 0.6	0.6 $\pm$ 0.6
MFI of Monocytes	294.6 $\pm$ 148.9	210.3 $\pm$ 101	192.7 $\pm$ 78
% of Neutrophils	42.7 $\pm$ 9.6	41.5 $\pm$ 9.8	40.1 $\pm$ 12.5

The table illustrates the results from the first round of flow cytometry examination of WO-2 and secondary antibody staining, involving the percentages of lymphocytes, monocytes, and neutrophils in the blood, the percentage of A $\beta^{++}$  monocytes and mean fluorescent intensity of total monocytes in 150 participants (78 CU, 36 MCI, and 36 AD-dementia). Data is presented as Mean  $\pm$  SD.

burden less than or equal to 25 CL, which was classified as the normal brain A $\beta$  group. Table 1 displays their corresponding APOE genotypes, clinical classifications, CL values, cognitive function scores, and composite scores. Table 2 summarizes the percentages of lymphocytes, monocytes, and neutrophils, as well as the percentage of A $\beta^{++}$  monocytes and the fluorescence intensity of the secondary antibody for total monocytes. Table 3 elaborates on the percentages of lymphocyte subsets and monocyte subsets, as well as the percentage of A $\beta^{++}$  monocytes and the fluorescence intensity of the secondary antibody for monocyte subsets.

**Differences in monocyte surface A $\beta$  between CU, MCI, and AD-dementia.** We first examined the percentage of A $\beta$ -binding monocytes based on clinical classification. The results demonstrated a 43% decrease in the percentage of A $\beta^{++}$  monocytes in total monocytes in AD-dementia patients compared to CU individuals (One-way Kruskal-Wallis test (2, 147) = 9.487,  $P < 0.0001$ , multiple comparisons test MCI vs. CU  $Z = 2.877$ ,  $DF = 147$ , adjusted  $p = 0.0080$ , AD-dementia vs. CU  $Z = 4.257$ ,  $DF = 147$ ,  $p < 0.0001$ , MCI vs. AD-dementia no significance, Fig. 5a).

In addition, we analyzed the fluorescence intensity of the secondary antibody for monocytes based on clinical classification. The results indicated a significant reduction in monocyte surface A $\beta$  levels in the AD-dementia group compared to the CU group. Specifically, there was a notable 26% decrease in monocyte surface A $\beta$  levels in AD-dementia patients compared to CU individuals (One-way Kruskal-Wallis test (2, 147) = 17.78,  $P = 0.0001$ , multiple comparisons test MCI vs. CU  $Z = 3.148$ ,  $DF = 147$ , adjusted  $p = 0.0033$ , AD-dementia vs. CU  $Z = 3.656$ ,  $DF = 147$ , adjusted  $p = 0.0005$ , MCI vs. AD-dementia no significance, Fig. 5i).

Our investigation also revealed significant differences in the percentage of NK cells, the percentage of intermediate monocytes, and the percentage of classical monocytes across the MCI, AD-dementia patients, and CU individuals (Supplementary Fig. 9).

**Correlation between monocyte surface A $\beta$  and A $\beta$ -PET burden.** We further investigated the correlation between monocyte surface A $\beta$  and A $\beta$  PET scoring. Firstly, we examined the association between the percentage of A $\beta$ -binding monocytes and A $\beta$  PET scoring. The results showed a negative correlation between the percentage of A $\beta^{++}$  monocytes and CLs (Spearman correlation  $r = -0.24$ ,  $P = 0.0038$ , Fig. 5b).

We then explored the relationship between the fluorescence intensity of the secondary antibody for monocytes and A $\beta$  PET scoring. The findings suggested a weak negative relationship between the fluorescence intensity and CLs (Fig. 5j). Although the Spearman coefficient ( $r$ ) value was around  $-0.2$ , this correlation was statistically significant ( $P = 0.0224$ ).

**Table 3 | Table demonstrates the results from the second round of flow cytometry examination of WO-2 and secondary antibody staining, together with CD14, CD16, CD45 antibodies, involving the percentages of lymphocyte subtypes, such as NK cells and T&B cells, and monocyte subsets, including intermediate, classic and non-classic monocytes, and percentage of A $\beta$ <sup>+</sup> monocytes in the monocyte subsets, and mean fluorescent intensity of the monocyte subsets in 113 participants (64 CU, 25 MCI, and 24 AD-dementia)**

Tube of WO-2 + 2nd and CD14, CD16, CD45	CU (n = 64)	MCI (n = 25)	AD-Dementia (n = 24)
<b>1) Lymphocyte subtypes:</b>			
% of NK cells (CD45 <sup>+</sup> CD14 <sup>+</sup> CD16 <sup>+</sup> )	17.8 ± 8	17.4 ± 5.2	12.7 ± 7.5
% of T&B cells (CD45 <sup>+</sup> CD14 <sup>+</sup> CD16 <sup>+</sup> )	82.2 ± 8	82.6 ± 5.2	87.3 ± 7.5
<b>2) Monocyte subsets:</b>			
% of Intermediate Monocytes (CD45 <sup>+</sup> CD14 <sup>+</sup> CD16 <sup>+</sup> )	7 ± 4.5	5.9 ± 2.4	4.9 ± 2.7
% of A $\beta$ <sup>+</sup> Intermediate Monocytes	3.5 ± 4.7	2.1 ± 2.7	2.9 ± 3.9
MFI of Intermediate Monocytes	434.3 ± 423.7	320.5 ± 278.7	416.4 ± 352.3
% of Classic Monocytes (CD45 <sup>+</sup> CD14 <sup>+</sup> CD16 <sup>+</sup> )	47 ± 16.4	48.3 ± 11.8	58.3 ± 12.3
% of A $\beta$ <sup>+</sup> Classic Monocytes	0.23 ± 0.32	0.18 ± 0.3	0.15 ± 0.22
MFI of Classic Monocytes	163.7 ± 100	143.2 ± 89.5	138.2 ± 59.4
% of Non-classic Monocytes (CD45 <sup>+</sup> CD14 <sup>+</sup> CD16 <sup>+</sup> )	14.2 ± 6.8	12.2 ± 6.2	12.9 ± 6.9
% of A $\beta$ <sup>+</sup> Non-classic Monocytes	0.35 ± 0.93	0.16 ± 0.45	0.12 ± 0.28
MFI of Non-classic Monocytes	104.8 ± 101.2	90.2 ± 66.8	101.5 ± 62.2

Data is presented as Mean ± SD.

Notably, the significance of the correlation diminished when considering monocyte subsets (Supplementary Fig. 10–12). This is likely because the classification of monocyte subsets led to cell numbers being spread thin, resulting in insufficient sample size to detect within each subset.

#### Correlation between monocyte surface A $\beta$ and cognitive decline.

Cognitive decline is a key clinical feature of AD. To investigate the relationship between monocyte surface A $\beta$  and cognitive function, we conducted various cognitive assessments focusing on executive function, attention, language, and episodic memory (EM). We also used two composite scores, the clinical dementia rating (CDR), and the preclinical Alzheimer cognitive composite (PACC). The results revealed positive correlations between the percentage of A $\beta$ <sup>+</sup> monocytes and cognitive scores, as well as the fluorescence intensity of the secondary antibody for monocytes and cognitive scores, except for a negative correlation with CDR (Fig. 5c–h, k–p). Spearman correlation coefficient (*r*) values, ranging from 0.2 to -0.4, indicated a moderate correlation. Importantly, all *r* values demonstrated statistical significance (*P* < 0.05).

**Implication of monocyte surface A $\beta$  as a biomarker for predicting brain A $\beta$ .** Finally, we evaluated the diagnostic potential of monocyte surface in predicting brain A $\beta$  levels. Using a multivariate generalized linear model, both the percentage of A $\beta$ <sup>+</sup> monocytes and the fluorescence intensity of the secondary antibody for monocytes remained significant after adjusting for age and *APOE*  $\epsilon$ 4 allele status (0/1/2). The coefficient *t*-scores and *P*-values were -2.835 and 0.0053, and -2.783 and 0.0062, respectively.

Subsequently, a panel comprising four biomarkers -- the percentage of A $\beta$ <sup>+</sup> monocytes, the percentage of A $\beta$ <sup>+</sup> NK cells, the percentage of A $\beta$ <sup>+</sup> classical monocytes, and the percentage of classic monocytes -- outperformed other examined biomarker combinations. This panel was used as a candidate tool to distinguish individuals whose brain A $\beta$ -PET burden was more than 25 CL from those whose were less than or equal to 25 CL. After adjustments for age, sex, years of education, and *APOE* genotype, the resulting area under the curve (AUC) of the new panel was 0.871 (CI: 0.803 to 0.938).

When compared to the basic panel, which relied solely on demographic characteristics (i.e., age, sex, years of education, and

*APOE* genotype), the AUC was calculated to be 0.808 (CI: 0.721 to 0.895). Upon integrating monocyte surface A $\beta$  biomarkers, the discrimination performance for AD significantly improved, approaching statistical significance (DeLong test *P* = 0.059, Fig. 5q). The new panel demonstrated a moderate sensitivity of 0.65 (CI: 0.524 to 0.758), and an impressive specificity of 0.976 (CI: 0.877 to 0.999). Figure 5r visually demonstrates the improved precision and recall metrics achieved by the new panel compared to the basic panel.

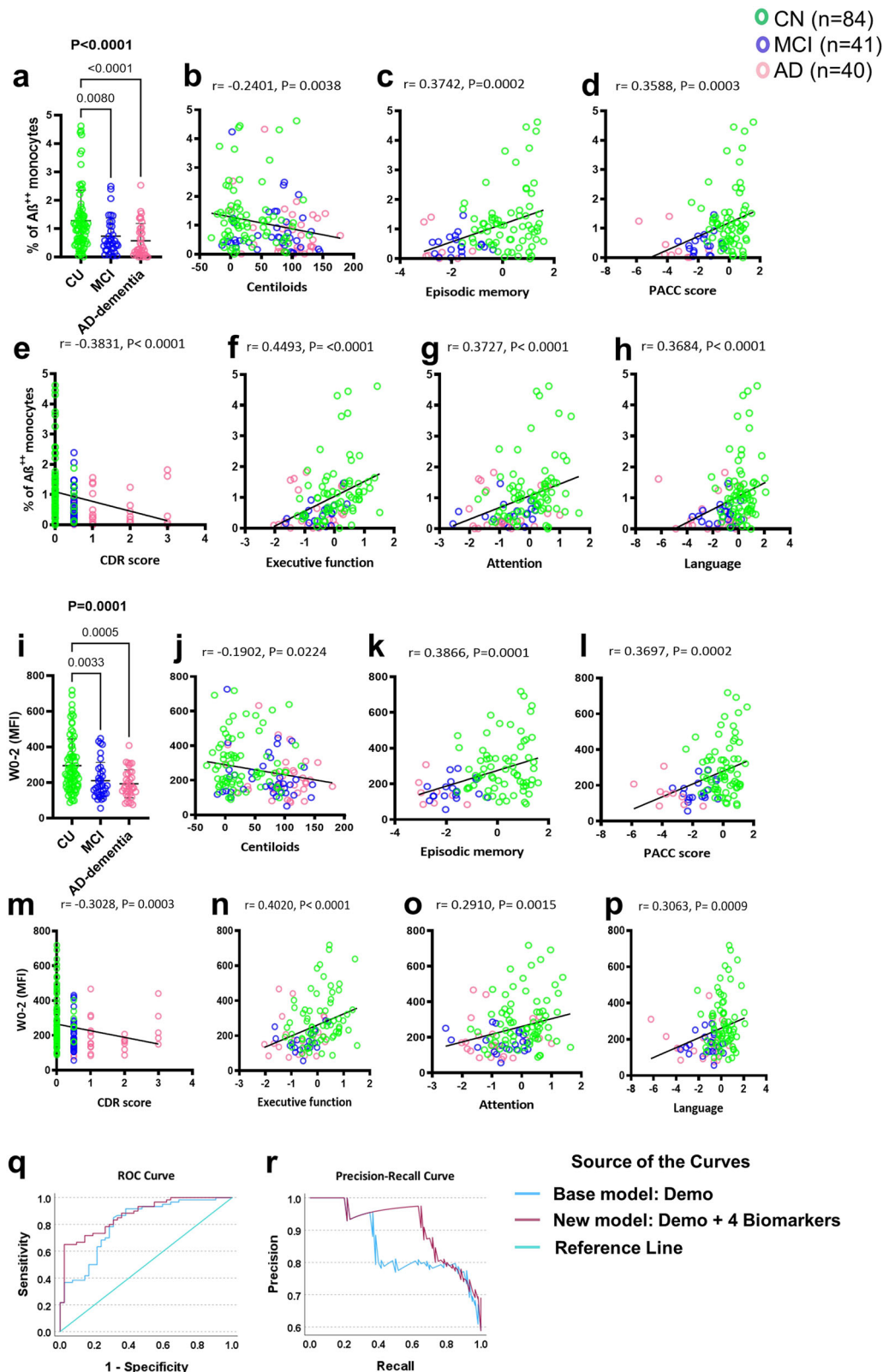
#### Altered surface A $\beta$ among CU with high brain A $\beta$ -PET burden.

Although there were no statistically significant differences between the CU - ve and CU + ve groups, we observed that many CU participants exhibited low surface A $\beta$  levels overlapping with the MCI and AD-dementia groups. We compared CU individuals based on brain A $\beta$ -PET status (CU-ve:  $\leq$  25 CL, *n* = 49; CU + ve:  $>$  25 CL, *n* = 29), MCI + ve (*n* = 27), and AD-dementia (*n* = 36), excluding those with MCI-ve (*n* = 9) from the comparison. The results indicated that CU+ve individuals had a percentage of A $\beta$ <sup>+</sup> monocytes lower than that of CU-ve individuals and similar to that of MCI +ve/AD-dementia across all three monocyte subsets (Supplementary Table 2 and Supplementary Figs. 13a, 14a, c, e).

Conversely, CU + ve individuals exhibited slightly elevated surface A $\beta$  fluorescent intensity compared with CU - ve individuals, and this intensity decreased in MCI + ve/AD-dementia individuals in total monocytes and classic monocytes, representing an inverted U-shaped pattern (Supplementary Table 2 and Supplementary Figs. 13b, 14d). However, this phenomenon was not observed in the CU + ve groups of the intermediate and non-classic monocytes (Supplementary Fig. 14b, f). In addition, CU + ve individuals showed a slightly elevated percentage of NK cells in total lymphocytes compared with CU - ve individuals, which returned to normal levels in MCI + ve and decreased in AD-dementia (Supplementary Table 2 and Supplementary Fig. 15a).

The decreased A $\beta$ <sup>+</sup> monocytes, increased surface A $\beta$  intensity, and increased percentage of NK cells (i.e., decreased percentage of T&B cells) may indicate an early dysregulation in CU + ve individuals. The percentage changes in monocyte subsets appeared to follow a linear pattern (Supplementary Table 2 and Supplementary Fig. 15b–d) without the inverted U-shaped pattern described above.





### Investigating monocyte infiltration into CSF and potential brain migration

To demonstrate the presence of peripheral monocytes entering the CSF and potentially the brain -- identified by the CD45, a pan-peripheral leukocyte surface marker; we investigated CSF pellet cells involving 15 samples (2 AD-dementia, 2 MCI, and 11 CU). The findings indicated that the presence of peripheral lymphocytes and monocytes in the CSF

is not unique but rather, occurs in all participants, regardless of clinical classification. In addition, the CSF CD45<sup>+</sup> cell composition is distinct from the peripheral. The preliminary results indicated an average of  $994 \pm 413$  cells/mL in the 15 CSF samples, comprising  $61 \pm 13.6\%$  CD45<sup>+</sup> peripheral immune cells and  $39 \pm 13.6\%$  CD45<sup>-</sup> cells. Among CD45<sup>+</sup> cells, an average of  $238 \pm 133$  lymphocytes/mL and  $86 \pm 73$  monocytes/mL were detected (Fig. 6a, a typical case). Most lymphocytes were

**Fig. 5 | Peripheral monocyte surface A $\beta$  as a potential biomarker for AD.**

Quantifying A $\beta$  on peripheral monocytes may serve as a non-invasive biomarker for AD. Our study included 150 participants (78 CU, 36 MCI, 36 AD-dementia). **a–p** A decrease in the percentage of A $\beta^{++}$  monocytes in MCI and AD-dementia compared to CU. Fluorescence intensity also showed a decrease in MCI and AD-dementia. A negative correlation was observed between the percentage of A $\beta^{++}$  monocytes and brain A $\beta$ -PET burden. Similarly, fluorescence intensity is weakly correlated with the A $\beta$ -PET burden. Correlations between the percentage of A $\beta^{++}$  monocytes, fluorescence intensity, and cognitive function were also observed, showing moderate

correlations. The datasets were not normally distributed, and *P*-values were determined using the Kruskal-Wallis test, followed by Dunn's multiple comparisons test (solid zig-zag line). The column dot plots represent mean  $\pm$  standard deviation. Correlation coefficients (*r*) and *P*-values were calculated using Spearman correlation analysis. **q, r** A multivariate model revealed the potential of monocyte surface A $\beta$  in predicting brain A $\beta$ -PET burden, with a panel of %A $\beta^{++}$  monocytes, %A $\beta^{+}$  NK cells, %A $\beta^{++}$  classical monocytes, and %classic monocytes performing best (AUC = 0.871). The new panel significantly improved AD discrimination, with a sensitivity of 0.65 and specificity of 0.976.

CD3<sup>+</sup> T cells (64.6  $\pm$  16.1%), primarily consisting of 73  $\pm$  10.8% CD4<sup>+</sup> T helper cells, and 18.3  $\pm$  9.5% CD8<sup>+</sup> cytotoxic T cells (Fig. 6i). In contrast to the peripheral, B cells (CD45<sup>+</sup>CD19<sup>+</sup>), NK cells (CD45<sup>+</sup>CD16<sup>+</sup> lymphocytes), and neutrophils (CD45<sup>+</sup>CD15<sup>+</sup>) were present in small quantities. CSF monocytes mainly comprised of CD14<sup>+</sup>CD16<sup>+</sup> intermediate monocytes, constituting 89.4  $\pm$  8% of total monocytes (Fig. 6c). In contrast to peripheral monocytes, non-classical and classical monocytes accounted for only 5.2  $\pm$  6.1% and 5.4  $\pm$  6.3%, respectively. A pie chart illustrates the CSF cellular composition, with 17.57  $\pm$  7.84% CD3<sup>+</sup>CD4<sup>+</sup> T cells, 4.91  $\pm$  3.4% CD3<sup>+</sup>CD8<sup>+</sup> T cells, 12.29  $\pm$  6.47% intermediate monocytes, 0.55  $\pm$  0.27% non-classical monocytes, 0.63  $\pm$  0.46% classical monocytes, 1.11  $\pm$  0.28% neutrophils 39  $\pm$  13.6% CD45<sup>-</sup> cells, and debris (Fig. 6j).

Due to the limited cell numbers, we only characterized CSF monocytes using part of the markers that applied to peripheral monocytes. The findings revealed that major CSF monocyte populations were positive for CX3CR1 (89.7  $\pm$  8.3%), double positive for Lin-1 and HLA-DR (72.8  $\pm$  10.2%), and double positive for CD11b and CD11c (80.4  $\pm$  11.3%); with 54.2  $\pm$  20% co-expressing CX3CR1 and CCR2, and 75.9  $\pm$  14.7% co-expressing CD14 and CD163 (Fig. 6d–g).

In addition, CSF monocytes showed surface A $\beta$  binding compared to lymphocytes (red cycle in Fig. 6h). In addition, three western blots of CSF pellet cell samples all affirmed the existence of A $\beta$  peptides (Suppl. Fig. 16). Furthermore, most CSF monocytes expressed CD68 and TREM2 (Fig. 6k, l).

To investigate the potential entry of CSF monocytes into the brain, post-mortem brain samples from two motor neuron disease patients were examined (*n* = 3, 1 patient with front cortex and temporal cortex, the other with temporal cortex only). The initial findings confirmed the presence of CD45<sup>+</sup>CD14<sup>+</sup>CD16<sup>+</sup> monocytes in the examined brain samples (Supplementary Fig. 17). Results showed that the most populated brain resident monocyte is the CD14<sup>+</sup>CD16<sup>+</sup> monocyte (57.8  $\pm$  1.7%); the CD14<sup>-</sup>CD16<sup>+</sup> and the CD14<sup>-</sup>CD16<sup>-</sup> accounted for 21.4  $\pm$  1.9% and 2.1  $\pm$  0.9%, respectively, which is consistent to CSF results. Due to high levels of autofluorescence in brain cells, additional markers such as CX3CR1 were used to distinguish the monocytes/macrophages in the brain (Supplementary Fig. 17).

**Peripheral migration of injected PBMCs in AD model mice**

The presence of A $\beta$ -binding monocytes in the CSF confirms their ability to enter the CNS. We further investigated whether these CSF peripheral monocytes can exit the CNS. Our investigation aimed to determine whether CSF-infiltrated peripheral leukocytes have the capability to migrate out of the CNS, providing insights into the entry and exit mechanisms of these immune cells between the CSF and periphery. To investigate whether infiltrated peripheral leukocytes possess the ability to migrate out of the CNS, CFSE-labeled C57BL/6 mouse PBMCs or Cx3CR1-eGFP mouse PBMCs were injected into the lateral ventricles of APP/PS1 (AD model) mouse brains. The aim was to examine whether these monocytes could re-enter the periphery through venous and lymphatic drainage pathways. The results indicated that the introduced PBMCs or monocytes were present in the blood and/or deep cervical lymph nodes (dcLN) in 15 out of 17 AD mice (88%, Supplementary Table 1) two days post

intracerebroventricular injection (Fig. 7d–l). Among these mice, the detection rate was 80% in young mice aged 15–35 weeks (*n* = 10), and 100% in older mice aged 68–80 weeks (*n* = 7). The detection rates in both blood and dcLN were equal at 71%. The A $\beta$  peptides carried by the CX3CR1<sup>+</sup> monocytes were detected using Qdot655-conjugated W0-2 mAb (Fig. 7f, l). Brain tissues were utilized for quality control (Fig. 7a–c).

In addition, we conducted further experiments by injecting fluorescent beads into the ventricles of three APP/PS1 mice, and none of the beads were detected in either the circulation or lymph nodes (see Supplementary Table 1 and Suppl. Fig. 18), indicating that the cell migration observed is a physiological process.

**Discussion**

This study developed a flow cytometry-based assay to identify CD14<sup>+</sup>CD16<sup>+</sup> monocytes binding to A $\beta$  in the blood, revealing a macrophage-like phenotype with high A $\beta$  phagocytic potential. Surface A $\beta$  levels on monocytes were significantly lower in MCI and AD-dementia patients compared to CU, suggesting impaired brain A $\beta$  clearance in AD. Using human CSF pellet cells and the APP/PS1 mouse model, the study demonstrated monocyte infiltration from the blood into the CSF, potentially into the brain, and peripheral monocytes exit from the CNS. The findings suggest that peripheral monocytes play a significant role in A $\beta$  clearance and that monocyte surface A $\beta$  could potentially serve as a blood-based biomarker for AD diagnosis and therapeutic effect monitoring.

Brain A $\beta_{1-42}$  are drained into the cerebral venous blood<sup>14</sup> and lymphatic system<sup>15</sup>, initially existing as free A $\beta$  until it binds to protein chaperones like lipoproteins and albumin<sup>16</sup>. Moreover, the volumetric dilution factor between CSF (140–270 mL) and plasma (~2800 mL) differs roughly by 15-fold. In contrast, the concentration of A $\beta_{42}$  in CSF (90 ng/L) is about 30-fold higher than that in plasma (30 ng/L)<sup>17–20</sup>. This 2-fold difference in the dilution factor implies that the “missing A $\beta_{1-42}$ ” is sequestered in a compartment distinct from plasma, suggesting the existence of an undefined A $\beta$  pool. While erythrocytes have been found to bind A $\beta$ <sup>21,22</sup>, other cell types, such as monocytes<sup>8</sup>, are more likely to be involved in eliminating A $\beta$  within the lumen of cerebral veins and transporting A $\beta$  in the blood.

We hypothesize that peripheral monocytes also enter the brain to complete A $\beta$  phagocytosis, as we have previously shown that innate phagocytosis can be inhibited by as little as 1% serum<sup>23</sup>. Therefore, it is unlikely that monocytes could efficiently clear A $\beta$  in the blood. This hypothesis is supported by studies suggesting the brain parenchyma infiltration of peripheral CD45<sup>high</sup>Ly6C<sup>high</sup> monocytes<sup>24</sup>, CD45<sup>high</sup>CD115<sup>+</sup> monocytes<sup>10</sup>, or CD45<sup>+</sup>CD163<sup>+</sup> monocytes<sup>25</sup> in reducing brain A $\beta$  plaque load.

The presence of CD45<sup>+</sup>CD163<sup>+</sup>CD14<sup>+</sup>CD16<sup>+</sup> monocytes in the CSF with high surface A $\beta$  binding, as shown in this study, indicates their active role in A $\beta$  clearance in the brain. Potential sites for the entry of peripheral monocytes into the brain include the choroid plexus, meninges, and perivascular spaces of aged AD mice<sup>24</sup>. The mechanism triggering this cellular ingress pathway in AD remains unclear, but an interferon  $\gamma$ -dependent recruitment of monocytes to the brain upon programmed death-1 blockade

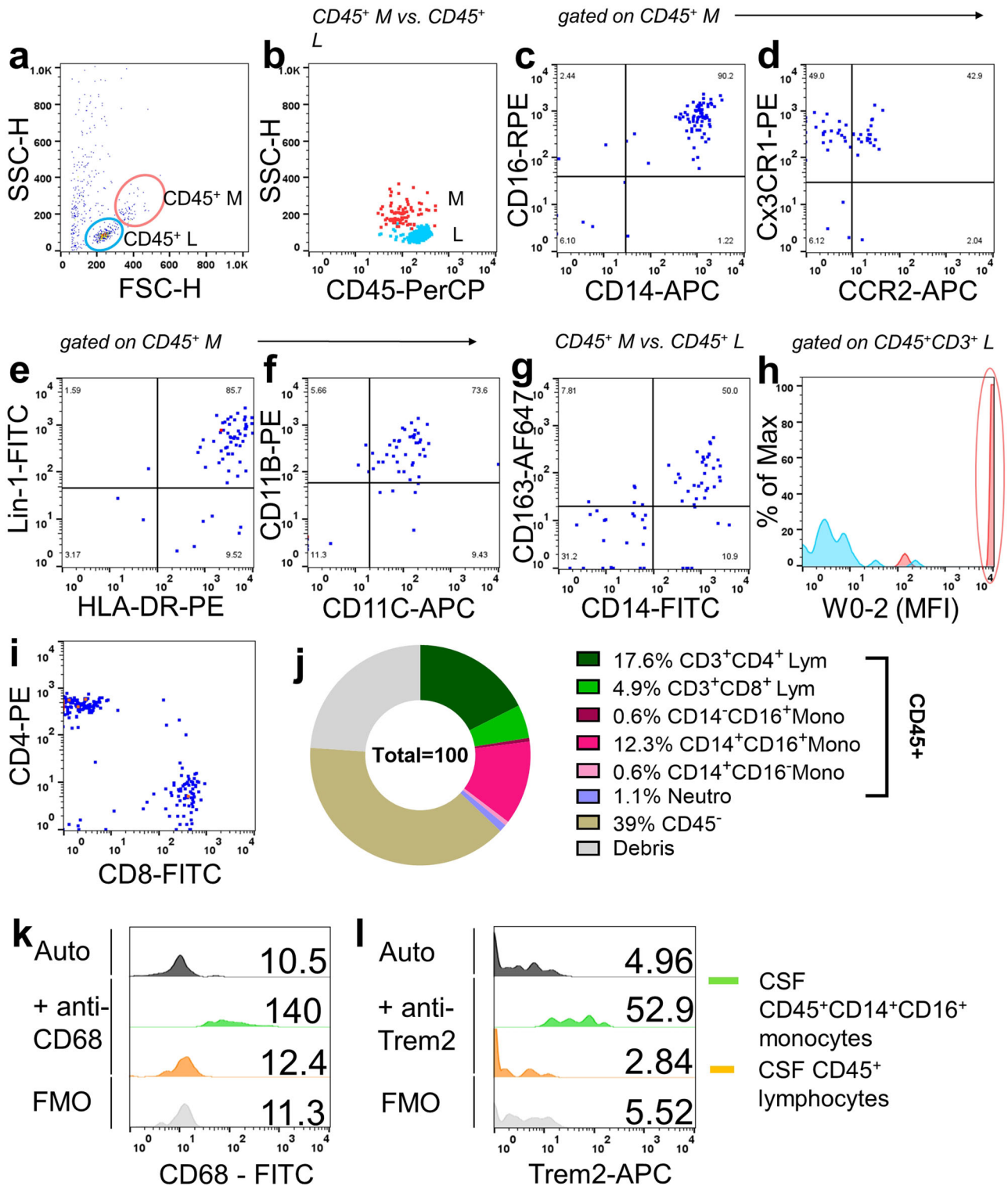
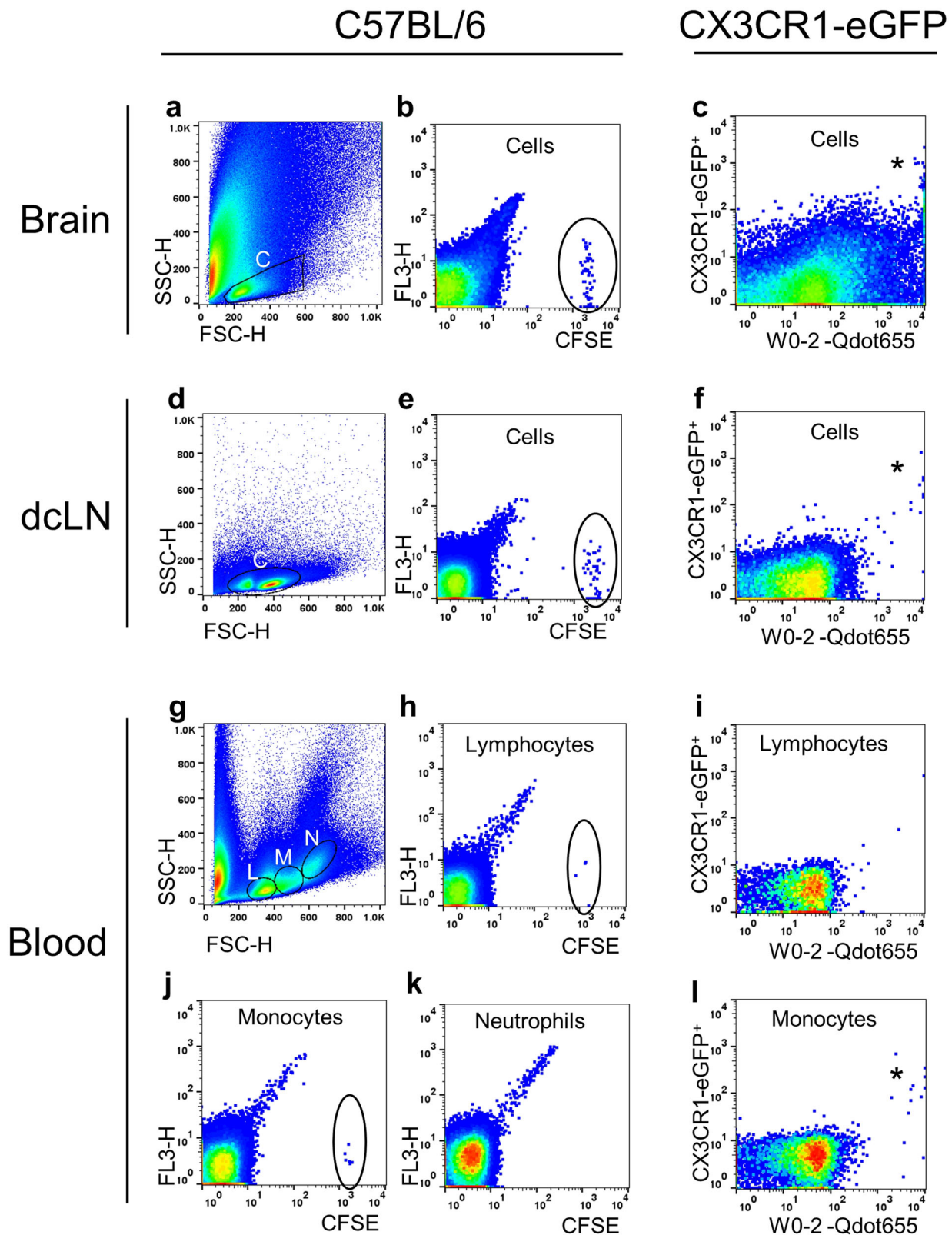


**Fig. 6 | Investigating monocyte infiltration into CSF.** To demonstrate the presence of peripheral monocytes entering the CSF, CSF pellet cell samples from 15 participants (2 AD-dementia, 2 MCI, and 11 CU) were investigated. **a, b** Presence of peripheral lymphocytes and monocytes, identified by CD45, a pan-peripheral leukocyte surface marker, in the CSF occurred in all participants, regardless of clinical classification. **c-h** CSF monocytes expressed CD14, CD16, CX3CR1, Lin-1, HLA-DR,

CD11b, CD11c, and CD163. In addition, they showed surface A $\beta$  binding compared to lymphocytes. **i** Within CSF CD3<sup>+</sup> lymphocytes, the presence of CD4<sup>+</sup> or CD8<sup>+</sup> T cells was identified. **j** A visual representation of the CSF cellular component was illustrated in a pie chart. **k, l** Furthermore, most CSF monocytes expressed CD68 and TREM2. Auto: Autofluorescence. Numbers within the histogram represent the mean fluorescence intensity (MFI). FMO = fluorescence minus one.

has been proposed<sup>26</sup>. In addition, a recent study proposes that arachnoid cuff exit (ACE) points enable fluid and molecule exchange between the subarachnoid space and dura mater, supporting cellular trafficking during neuroinflammation<sup>27</sup>.

We hypothesize that peripheral monocytes leave the brain and return to the blood after completing A $\beta$  phagocytosis via a specific cellular egress pathway. Two recent studies have shown how CSF exchanges with the glymphatic system to remove waste, including A $\beta$ ,



from the brain<sup>28,29</sup>. In this study, the injection of PBMCs into the brain ventricles and their detection in the blood and lymph nodes provide first-hand evidence for the potential return of these infiltrated monocytes to the periphery. Our findings are even more significant as we have demonstrated not only the exchange of fluids and molecules but also the trafficking of immune cells via this cellular ingress and egress system in AD.

Genome-wide association studies have implicated disruptions in phagocytosis and endocytosis pathways<sup>30,31</sup> to late-onset AD, consistent with our findings of altered monocyte phagocytosis<sup>9</sup>. Our investigation of peripheral monocytes in AD showed significant changes in surface markers, suggesting peripheral immune responses, although the exact reasons remained unknown<sup>32</sup>. In this study, we observed elevated expression of CCR2, CD68, and TREM2 in A $\beta$ -

**Fig. 7 | Detection of Adoptive PBMCs in Blood and Deep Cervical Lymph Nodes.** PBMCs were sourced from donor C57BL/6 mice and labeled with CFSE ( $n = 13$ ) or from CX3CR1-eGFP mice without CFSE labeling ( $n = 5$ ). Both sets of PBMCs were injected into the lateral ventricles of APP/PS1 mice between 15 and 80 weeks of age. Two days later, recipients' brains, deep cervical lymph nodes (dCLN), and blood were examined using fluorescent flow cytometry. **a, d, and g** display typical flow cytometry light scatter dot plots of the brain, dCLN, and blood, respectively. The presence of donors' CFSE<sup>+</sup> cells in the recipients' brains confirmed successful delivery (circled in **b**). Likewise, CFSE<sup>+</sup> cells in recipients' dCLN (circled in **e**) and

blood (circled in **h, j**) validated peripheral migration. No CFSE<sup>+</sup> cells were found in the recipients' blood neutrophil gating (**k**). Notably, the donors' CX3CR1-eGFP<sup>+</sup> monocytes were identified as carrying substantial amounts of A $\beta$  in the recipients' brain (asterisked in **c**), dCLN (asterisked in **f**) and blood (asterisked in **l**). A few CX3CR1-eGFP<sup>+</sup> monocytes were found in the recipients' blood lymphocyte gating (**i**) due to an overlap between lymphocytes and monocytes. This flow cytometry analysis demonstrates the migration and A $\beta$ -carrying capabilities of adoptive PBMCs in different tissues. C: Cells; L: Lymphocytes; M: Monocytes; and N: Neutrophils.

binding monocytes in the blood. Most CSF monocytes were intermediate (CD14<sup>+</sup>CD16<sup>+</sup>) monocytes, a subset not commonly found in peripheral monocytes, and expressed CD68 and TREM2, resembling tissue macrophages and microglia. This suggests that perivascular or CSF monocytes may contribute to the pool of A $\beta$ -binding monocytes in the blood. The upregulation of CD68 and TREM2 in CSF monocytes may result from the unique perivascular and CSF environment, lacking serum but containing A $\beta$ , highlighting the association of TREM2 with AD<sup>33</sup>.

In a study involving 252 participants from AIBL, AD patients exhibited a 16% reduction in plasma A $\beta$ <sub>1-42</sub> compared to healthy controls<sup>20</sup>. The plasma A $\beta$ <sub>1-42</sub>/A $\beta$ <sub>1-40</sub> ratio, phosphorylated-tau181, glial fibrillary acidic protein, and neurofilament light were also evaluated as potential blood biomarkers for AD<sup>34</sup>. In addition to plasma A $\beta$  diagnostics for AD, our findings highlight the potential use of blood cell-based A $\beta$  diagnostics. The correlation between the reduction in A $\beta$ -carrying monocytes in AD patients and their association with brain A $\beta$  burden and cognitive decline underscores the clinical relevance of our study, emphasizing the potential for these markers to enhance AD diagnosis and prognosis.

To address concerns about potential BBB damage from cell injections and the presence of these cells in circulation, our data showed minimal counts of injected beads in the periphery, suggesting it is a physiological event with limited migration via BBB leakage. In addition, limitations such as the difficulty in obtaining CSF samples from AD patients compared to blood samples resulted in a small study cohort. While the improvement in our model's performance (AUC 0.87 vs 0.81) is marginal, we find the diagnostic potential of A $\beta$ -binding monocytes in peripheral blood promising, emphasizing the need for further validation to confirm their utility.

In this study, we observed that surface A $\beta$  levels on monocytes were significantly lower in MCI and AD-dementia compared to CU, suggesting impaired brain A $\beta$  clearance. We also showed that CD45<sup>+</sup>CD163<sup>+</sup>CD14<sup>+</sup>CD16<sup>+</sup> monocytes actively clear A $\beta$  in the CSF. Importantly, our study provided direct evidence of monocytes leaving the brain and re-entering the bloodstream. These findings highlight the importance of understanding these cellular processes in AD. Such insights could pave the way for developing treatments that enhance A $\beta$  clearance by promoting monocyte A $\beta$  phagocytosis, thereby advancing our understanding and treatment of AD.

## Methods

### The flow cytometry-based assay

To accurately identify monocytes in the blood that strongly bind to A $\beta$ , we first compared several anti-human A $\beta$  monoclonal antibodies for their ability to identify A $\beta$ -binding monocytes in the blood. 100  $\mu$ L anti-coagulated peripheral whole blood from six individuals (3 CU, 2 MCI and 1 AD-Dementia) were stained with various anti-A $\beta$  antibodies and an anti-APP antibody -- 20  $\mu$ g/mL W0-2, 40  $\mu$ g/mL 4G8 or 20  $\mu$ g/mL 6E10 (kindly provided by Dr Qiao-Xin Li), 20  $\mu$ g/mL 22C11 (Sigma-Aldrich), with the optimal concentrations determined by antibody titrations, incubated on a shaker, protected from light, at room temperature for 15 min. Afterward, the blood sample was washed twice using phosphate buffer saline (PBS), centrifuged at 300  $\times$  *g* for 5 min to

remove the unbound antibody, and subsequently incubated with 10  $\mu$ g/mL FITC-conjugated donkey anti-mouse IgG (H + L) (Jackson Laboratories) for 15 min. Then, red blood cells were lysed, and leukocytes were fixed using 2 mL BD FACS Lysing Solution (BD Biosciences) for 10 min. Cells were washed with 2 mL PBS, pelleted by centrifugation, resuspended in 100  $\mu$ L PBS, incubated with RPE-conjugated anti-CD16 (Dako) and APC-conjugated anti-CD14 (BD) antibodies for another 15 min, then washed with 2 mL PBS, pelleted, resuspended with 0.5 mL PBS, and analyzed with a flow cytometer (BD FACSCalibur). The antibodies' performance was assessed by comparing the fluorescent intensity of the secondary antibody to sensitively identify A $\beta$ -binding monocytes within the monocytes; especially the monocyte subsets, which were classified based on CD14 and CD16 positivity.

After optimization, the final assay was determined to be: 100  $\mu$ L anti-coagulated peripheral whole blood stained with 20  $\mu$ g/mL W0-2, incubated on a shaker, protected from light, at room temperature for 15 min, washed twice with PBS, subsequently incubated with 10  $\mu$ g/mL Alexa Fluor<sup>®</sup> 488-conjugated goat anti-mouse IgG<sub>2a</sub> secondary antibody (Life Technologies) for 15 min, lysed and fixed with 2 mL FACS Lysing Solution (BD) for 10 min, washed with 2 mL PBS, pelleted by centrifugation, resuspended with 0.5 mL PBS, and analyzed with FACSCalibur. Stopped at 40,000 events and collected the remaining cells in the FACS tube by centrifugation. Cells were resuspended in 100  $\mu$ L PBS, incubated with RPE-conjugated anti-CD16 (Dako), PerCP-conjugated anti-CD45, and APC-conjugated anti-CD14 (BD) antibodies for another 15 min, then washed with 2 mL PBS, pelleted, and resuspended with 0.5 mL PBS, and reanalyzed with FACSCalibur. Auto-fluorescence, IgG<sub>2a</sub> isotype antibody, and secondary antibody alone were prepared for each sample.

### Confocal microscopy

Three CU PBMCs were stained with W0-2 and AF488-conjugated secondary antibodies, and two CU PBMCs were stained with RPE-CD16 and APC-CD14 antibodies, fixed and permeabilized, and stained with FITC-conjugated 6E10. A Leica SP8 confocal microscope was utilized to identify A $\beta$  in terms of W0-2 plus secondary antibody on the cell surface or 6E10 in the cytoplasm with Z-stack imaging. The confocal images were analyzed, and channels were merged using Fiji (ImageJ 1.51n, NIH, USA). The 3D view of cell surface A $\beta$  was generated using Imaris Viewer (Oxford Instruments).

### The synthesized A $\beta$ <sub>1-42</sub> incubation

To form oligomerized A $\beta$ <sub>1-42</sub>, synthesized A $\beta$ <sub>1-42</sub> powder (China Peptides, Shanghai) was dissolved in a solution of 90% DMSO and 10% 10 mM PBS (PH = 7.4), and preincubated at 4  $^{\circ}$ C overnight. 10  $\mu$ M oA $\beta$ <sub>1-42</sub> was added to a tube of 100  $\mu$ L peripheral whole blood from six CU individuals. DMSO was added to another tube of blood as vehicle control. Blood samples were incubated on a shaker at 37  $^{\circ}$ C for 15 min, washed three times with PBS, and stained with W0-2, secondary, CD16, CD45, and CD14 antibodies described as above.

### FACS Sorting

Human PBMCs were separated using Ficoll-Paque Plus (GE Healthcare) and were stained with FITC-conjugated CD14 and AF647-conjugated

CCR2 antibodies. CCR2 was used as a surrogate of W0-2 to identify blood A $\beta$ -binding monocytes as A $\beta$  was primed by W0-2 in the Western blot and SELDI-TOF Mass Spectrometry. The cells were then sorted into CCR2<sup>+</sup>CD14<sup>+</sup>, CCR2<sup>+</sup>CD14<sup>-</sup> monocytes, and CCR2<sup>-</sup>CD14<sup>-</sup> lymphocytes. The sorted populations were concentrated to 1  $\times 10^6$  cells/mL, and a protease inhibitor cocktail (cOmplete, Roche) was added before freezing.

### Western Blotting

Sorted PBMCs from 4 CU individuals were pooled to make two sets of cells with 1  $\times 10^6$  cells per cell type. Cells were ultrasonicated at 4 °C for 20 s, denatured within LDS sample buffer (ThermoFisher) at 90 °C for 5 min, and reduced by 50  $\mu$ M DTT. 24  $\mu$ L proteins and 7  $\mu$ L SeeBlue protein standard (Thermo Fisher) were loaded to 10-well NuPage gel (Thermo Fisher). Electrophoresis was conducted with an MES buffer at 100 V for 50 min. Proteins were transferred to a 0.2  $\mu$ m pore size nitrocellulose membrane (Bio-Rad) at 100 V for 35 min. Immunodetection was carried out using 1:1000 W0-2 antibody and 1:10,000 rabbit anti-mouse HRP conjugated IgG (Invitrogen), and ECL substrate (ThermoFisher).

### SELDI-TOF Mass spectrometry

2  $\mu$ L of 0.25 mg/mL W0-2 mAb was added to the spots of the PS10 ProteinChip array, and the chip was incubated in a humid chamber at 4 °C overnight. The antibody was removed and 5  $\mu$ L of blocking buffer (0.5 M ethanolamine in PBS) was added, the array was incubated for 30 min. The blocking buffer was removed, and each spot was washed with 200  $\mu$ L of 0.5% Triton X-100/PBS (wash buffer) for 5 min three times. The solvent was removed, and the spots were washed with 20  $\mu$ L of PBS for 5 minutes three times. Sorted cell lysates from two CU PBMCs were added to each spot; the array was incubated at room temperature for 2 h. The samples were removed, and each spot was washed twice with 200  $\mu$ L of wash buffer for 10 sec, followed by a wash with 200  $\mu$ L PBS twice for 10 s, and finally, the arrays were washed with 200  $\mu$ L 1 mM HEPES twice for 10 seconds. The array was air-dried. A volume of 1  $\mu$ L of sinapinic acid (SPA, 50% saturated in 50% (v/v) acetonitrile and 0.5% in TFA) was applied to each spot twice. The array was air-dried between each application. All the incubations and washes were performed on a shaking table. Chips were analyzed in a PBSiC, SELDI-TOF MS and peaks were analyzed using Ciphergen ProteinChip software 3.1.

### Triple-quadrupole mass spectrometry

For immunoprecipitation, 19  $\mu$ g of anti-A $\beta$  mAbs (clone 6E10 and clone 4G8 at a 1:1 ratio) was loaded onto ProteinG W columns. Columns were blocked with 25 mM dimethylpyrazole (DMP) and washed with PBS. Subsequently, 7.5  $\times 10^4$  sorted cells per cell type from three CU individuals were mixed with 20  $\mu$ L of urea 8 M and 80  $\mu$ L of PBS (0.5% CHAPS), sonicated, and loaded into columns. The columns were washed with PBS and then water. Samples were eluted using a mixture of 30% acetonitrile, 10% isopropyl alcohol, and 0.1% formic acid. After the speed vacuum, enzymatic digestion was performed. For digestion, samples were treated with urea protocol, followed by Lys-N digestion. Digested peptides were desalted using an Oasis HLB  $\mu$ Elution 96-well plate (Waters Corp). LC-ESI-QQQ-MRM assay was conducted using an Agilent 1200 Infinity series UHPLC system connected to 6495 triple-quadrupole MS (TQ-MS). Data processing involved Skyline software to extract peak areas for A $\beta$  peptides and derive light-to-heavy ratios by comparing them to stable isotope-labeled analogs.

### Four-color flow cytometry phenotyping scheme

A four-color flow cytometry scheme was used to phenotype A $\beta$ -binding monocytes in blood and CSF. For blood samples, Lin-1 and HLA-DR antibodies (BD) were tested together with CD45, W0-2 and secondary antibodies. CCR2, CD11b, CD11c, CD35/CR1, CD68, CD85A/

LILRB3, CD85D/LILRB2, CD91/LRP1, CD163, CX3CR1 (BD), MerTK, TREM2 (R&D Systems), and P2X7 (made in house) antibodies were tested together with CD14, CD16, W0-2 and secondary antibodies. At least three samples were tested for each antibody or antibody combination, with a total of 23 blood samples analyzed, regardless of clinical classification. For 14 CSF pellet cells, Lin-1, HLA-DR, CCR2, CD3, CD4, CD8, CD11b, CD11c, CD14, CD16, CD68, CX3CR1, TREM2, W0-2 and secondary antibodies were tested together with CD45 antibody.

### Two-Color Fluorescent Reporting System

To form oligomerized A $\beta_{1-42}$ , 0.5 mg synthesized A $\beta_{1-42}$  powder (China Peptides, Shanghai) was dissolved in 250  $\mu$ L 10 mM NaOH, diluted with 250  $\mu$ L ultrapure water, neutralized with 56  $\mu$ L 10X TBS pH 7.4 (ThermoFisher), and incubated at 37 °C overnight. A $\beta_{1-42}$  aggregates were collected with 16,000  $\times g$  centrifugation for 1 min, washed once with HBSS (ThermoFisher), collected with 16,000  $\times g$  centrifugation for 1 minute, resuspended with 200  $\mu$ L filtered 0.1 M NaHCO<sub>3</sub>, mixed with 36  $\mu$ L 10 mg/mL pHrodo red dye (ThermoFisher), incubated at room temperature for 1 h with rotation in the dark, collected with 16,000  $\times g$  centrifugation for 1 min, washed once with 1 mL methanol, washed three times with 1 mL HBSS, resuspended in 200  $\mu$ L HBSS, sonicated at room temperature for 10 min, and stored in aliquots at -80 °C for further use.

To prepare cell cultures, HT22 (Millipore, Cat. No: SCC129), U251 (Sigma-Aldrich, Cat. No: 09063001) and BV2 cells (provided by Professor Rosario Donato, University of Perugia) were cultured in RPMI 1640 media (ThermoFisher) with 10% FBS and 100 U/mL penicillin-streptomycin with T75 flasks until 90% confluency, trypsinized, pelleted at 300  $\times g$  for 5 min, resuspended with complete media, and plated in 1 mL to 35 mm cell culture dishes (Falcon) with 4  $\times 10^5$  cells/mL concentration, cultured overnight and changed to FBS-free RPMI 1640 media for further tests.

To prepare PBMCs, two tubes of anticoagulated blood were mixed, diluted with 15 mL PBS, carefully suspended on 15 mL Ficoll-Paque PLUS (Cytiva), and centrifuged with 400  $\times g$  for 30 min without brake. PBMCs were aspirated using a transfer pipette, washed with PBS, pelleted with 400  $\times g$  for 5 min, resuspended in 10 mL red cell lysis buffer at room temperature for 10 min, washed with PBS, pelleted with 400  $\times g$  for 5 min, resuspended in 200  $\mu$ L PBS, diluted with FBS-free RPMI 1640 media, and plated in 1 mL to 35 mm cell culture dishes with 5  $\times 10^5$  cells/mL concentration for further use.

To test cell phagocytosis, each dish of cells was given 5  $\mu$ L pHrodo red-conjugated oligomerized A $\beta_{1-42}$  with the gentle mix, incubated for multiple time points (0.5, 1, 2, 4, and 24 h). Cells were then collected with a cell scraper, washed once with PBS, pelleted with 300  $\times g$  for 5 min, resuspended in 100  $\mu$ L PBS, stained with 20  $\mu$ g/mL AF-647 Aducanumab (Biogen) at room temperature for 15 minutes, washed once with PBS, centrifuged, resuspended with 0.5 mL PBS, and analyzed using a flow cytometer (BD FACSCalibur).

### AIBL cohort study

A total of 150 Caucasian participants were randomly selected from the AIBL study: a longitudinal, prospective observational study integrating peripheral biomarkers with neuroimaging, neuropsychological assessments, and lifestyle data<sup>35</sup>. This study was conducted in Melbourne, Victoria and Perth, Western Australia, with our samples collected from the Melbourne site. The participants, comprising 73 males and 77 females, had a mean age of 75 and were fluent in English (Table 1). According to the AIBL Participant Consent Form (March 2020), no payments are made to participants in this study. However, all study participants are eligible for reimbursement of transportation costs incurred by traveling to and from clinic appointments and the cost of food if required to fast before a blood test. Participants will incur no expenses for any tests or procedures undertaken for study purposes. As per the NINCDS-ADRDA criteria, they were categorized

into three clinical groups: cognitively unimpaired controls (CU,  $n = 78$ ), mild cognitive impairment (MCI,  $n = 36$ ) or prodromal AD<sup>36,37</sup>, and AD-dementia (AD,  $n = 36$ )<sup>35,38</sup>. In addition, participants were stratified based on the A $\beta$ -PET neuroimaging results (as described below). Researchers remained blinded to all clinical and demographic information until completion.

A 3D T1-weighted MRI was obtained for screening and coregistration with the PET images. The PET methodology has been previously described<sup>39</sup>. All A $\beta$ -PET scans were spatially normalized using CapAIBL<sup>40</sup> and quantified using the Centiloid (CL) scale. The thresholds of A $\beta$ -PET positivity were selected based on postmortem studies that the individuals with A $\beta$ -PET load  $\geq 15$ CL and  $< 25$ CL may have sparse A $\beta$  plaques<sup>41,42</sup>.

The cognitive assessments have been extensively outlined and validated in prior research within the AIBL cohort<sup>43–46</sup>. In summary, the episodic memory composite includes the California Verbal Learning Test (Second Edition, CVLT-II), Logical Memory, and Rey Complex Figure Test. The preclinical Alzheimer cognitive composite (PACC) includes the California Verbal Learning Test (Second Edition, CVLT-II), Logical Memory, Digit Symbol Coding, and Mini-Mental State Examination (MMSE). These assessments served as robust and established measures in our study.

Peripheral whole blood was collected via venepuncture between 8:00 a.m. and 10:30 a.m. after overnight fasting. Whole blood was kept in EDTA anticoagulant Vacutainer<sup>®</sup> tubes (BD Biosciences) and kept on ice during transportation. Processing of whole blood was completed within three hours after collection.

By using the flow cytometry assay, we initially quantified the percentage of A $\beta$ -binding monocytes and the fluorescence intensity of the secondary antibody, which reflects the level of A $\beta$  on cell surfaces. Since this assay utilizes a secondary antibody, the W0-2 mAb cannot be used concurrently with other antibodies. Therefore, after restaining the cells with CD14 and CD16 antibodies, we quantified the percentage of A $\beta$ -binding monocytes and the fluorescence intensity of the secondary antibody based on the CD14 and CD16 classification of monocytes. Notably, only 113 samples from a total of 150 individuals were co-investigated with CD14, CD16, and CD45 antibodies. These samples were obtained from 64 CU, 25 MCI, and 24 AD-dementia individuals. The limited investigation of these antibodies was due to their introduction after the start of the AIBL cohort study.

FACS data was analyzed using Flow Jo V10 software (Flow Jo, LLC). The A $\beta^{++}$  monocyte data was analyzed based on clinical classification (CU, MCI, and AD-dementia) using one-way ordinary ANOVA or Kruskal-Wallis test if the data was not normally distributed, followed by multiple comparisons tests. Two-tail  $P$ -values were presented. Correlations were evaluated through nonparametric Spearman correlation analysis, exploring the relationship between the A $\beta^{++}$  monocytes and brain A $\beta$  levels or cognitive functions, respectively. All between-group comparisons and Spearman correlation analyses were executed and visually represented using GraphPad Prism (Version 9.2). In addition, ROC analysis and Precision-Recall analysis were conducted and graphically presented using IBM SPSS Statistics (Version 29.0).

### CSF Pellet cell collection

15 CSF pellet cell samples, nine males and five females with a mean age of 78 were collected from the AIBL study. This cohort included two individuals with AD, two with MCI, and 11 CU participants, of which seven were A $\beta$  PET<sup>+</sup> and eight were A $\beta$  PET<sup>-</sup>. Approximately 10 mL of CSF samples were obtained via lumbar puncture and then centrifuged at 300 g for 10 min at 4 °C. The resultant CSF pellet cells were resuspended in 200  $\mu$ L PBS and kept on ice during transportation. All processing of the CSF pellet cells was completed within three hours after collection.

### Fluorescence flow cytometry tracking of intraventricular injection of live mononuclear cells into peripheral blood and lymph

Twenty-one 15- to 80-week-old APP/PS1 (JAX APPsw, PSEN1dE9; 14 males and 7 females) mice used in this study were bred and housed with cage mates in a pathogen-free environment at the KMB Biosciences Facilities. Twenty-six 7-week-old female C57BL/6 donor mice were purchased from Ozgene. Peripheral blood was obtained from the C57BL/6 mice through cardiac puncture at a donor to recipient ratio of 2:1. Mononuclear cells were isolated via density centrifugation, labeled with carboxyfluorescein succinimidyl ester (CFSE, Abcam), and prepared for intraventricular injection. The APP/PS1 recipient mice were anesthetized using 2% isoflurane in the air to attain a surgical plane. Their heads were securely immobilized in a stereotaxic frame (RWD Life Science) with the application of eye lubricant. Pre-operative analgesia is administered, followed by a scalp incision and treatment of the skull with hydrogen peroxide to expose bregma. The cannulation site, located at 0.46 mm posterior and 0.8 mm lateral to bregma, was drilled, and 5  $\mu$ L of cells were injected into the lateral ventricle (2.25 to 2.5 mm below the bone surface) using a microinjection needle. The injection speed was set at 1  $\mu$ L/min, and the needle was retained for 10 min after injection to prevent leakage of the cells. The wound was closed with sutures. After a 2-day period, the recipient mice were anesthetized with isoflurane, peripheral blood was collected via cardiac puncture, and they were humanely killed by cervical dislocation. The brain was quickly removed, and the hippocampus and retrosplenial cortex were dissected and soaked in ice-cold PBS. The deep cervical lymph nodes (dcLNs) were severed from both sides beneath the sternomastoid muscles and soaked in ice-cold PBS. The blood underwent lysis using red blood cell lysis buffer. The dissected brain tissue and dcLNs were minced and filtered through a 100  $\mu$ m cell strainer using the plunger end of a 1 mL syringe. The cell strainer was continuously rinsed with ice-cold PBS. The lysed blood and homogenized samples were centrifuged at 300  $\times$  g and 4 °C for 5 min. The supernatant was carefully aspirated, and the pellets were resuspended in 100  $\mu$ L PBS and analyzed using a flow cytometer (BD FACSCalibur).

Eight 8- to 12-week-old CX3CR1-eGFP mice (JAX, 3 males, and 5 females) were utilized to collect CX3CR1-eGFP<sup>+</sup> monocytes for monocyte-specific tracking. These monocytes were injected into the recipients' lateral ventricles without CFSE labeling. After a two-day period, the recipient mice were euthanized, and tissues were collected. The lysed blood and homogenized brain and lymph node samples were centrifuged at 300  $\times$  g at 4 °C for 5 min. The supernatant was carefully discarded, and the pellets were resuspended in 100  $\mu$ L ice-cold PBS. To identify A $\beta$ -binding monocytes, 20  $\mu$ g/mL Qdot655-conjugated W0-2 mAb was added to the cell suspension, which was then incubated on ice for 20 min and washed once with PBS before analysis using a flow cytometer (BD FACSCalibur).

In addition, 6  $\mu$ m high-intensity alignment green beads (Polysciences) were injected into the lateral ventricle of three APP/PS1 mice (aged 32 weeks, 49 weeks, and 55 weeks) as a controlled study. Two days post-injection, peripheral blood, and dcLNs were collected to trace these fluorescent beads.

### W0-2 mAb Direct labeling

Directly labeling W0-2 mAb with a fluorescent dye caused high non-specific binding. To preserve the antibody's activity, a high-fidelity method was used, involving attaching dye molecules to heavy chain N-linked glycans. W0-2 mAb was directly labeled with RPE, Qdot525, and Qdot655 using the SiteClick labeling kits (Thermo Fisher). These fluorescently labeled antibodies were used in later stages of experiments.

### Ethical approval

The St Vincent's Hospital Melbourne Human Research Ethics Committee granted ethical approval for the human studies (Ref: HREC-A

028/06). Informed consent was obtained from all participants and caregivers.

Ethical approval for the animal study was granted by The Florey Animal Ethics Committees (Ref: 22–058).

### Reporting summary

Further information on research design is available in the Nature Portfolio Reporting Summary linked to this article.

### Data availability

Human participant data is available upon request through an AIBL EOI mechanism from the corresponding author, CM, via the link <https://aibl.org.au/collaboration/#data-access>. The data are not publicly available due to containing information that could compromise the privacy of research participants. The animal data that support the findings of this study are available via the link <https://figshare.com/s/4e7f588f527163643c5f>.

### References

1. Masters, C. L., Bateman, R., Blennow, K., Rowe, C. C., Sperling, R. A. & Cummings, J. L. Alzheimer's disease. *Nat. Rev. Dis. Prim.* **1**, 15056 (2015).
2. Villemagne, V. L. et al. Amyloid beta deposition, neurodegeneration, and cognitive decline in sporadic Alzheimer's disease: a prospective cohort study. *Lancet Neurol.* **12**, 357–367 (2013).
3. Mawuenyega, K. G. et al. Decreased clearance of CNS beta-amyloid in Alzheimer's disease. *Science* **330**, 1774 (2010).
4. Masters, C. L. et al. Neuronal origin of a cerebral amyloid: neurofibrillary tangles of Alzheimer's disease contain the same protein as the amyloid of plaque cores and blood vessels. *EMBO J.* **4**, 2757–2763 (1985).
5. Lewis, J. et al. Enhanced neurofibrillary degeneration in transgenic mice expressing mutant tau and APP. *Science* **293**, 1487–1491 (2001).
6. Selkoe, D. J. & Hardy, J. The amyloid hypothesis of Alzheimer's disease at 25 years. *EMBO Mol. Med.* **8**, 595–608 (2016).
7. De Strooper, B. & Karran, E. The cellular phase of Alzheimer's disease. *Cell* **164**, 603–615 (2016).
8. Michaud, J. P., Bellavance, M. A., Prefontaine, P. & Rivest, S. Real-time in vivo imaging reveals the ability of monocytes to clear vascular amyloid beta. *Cell Rep.* **5**, 646–653 (2013).
9. Gu, B. J. et al. Innate phagocytosis by peripheral blood monocytes is altered in Alzheimer's disease. *Acta Neuropathol.* **132**, 377–389 (2016).
10. Koronyo, Y. et al. Therapeutic effects of glatiramer acetate and grafted CD115(+) monocytes in a mouse model of Alzheimer's disease. *Brain* **138**, 2399–2422 (2015).
11. Ida, N. et al. Analysis of heterogeneous A4 peptides in human cerebrospinal fluid and blood by a newly developed sensitive Western blot assay. *J. Biol. Chem.* **271**, 22908–22914 (1996).
12. Kim, T. et al. Human LILRB2 is a beta-amyloid receptor and its murine homolog PirB regulates synaptic plasticity in an Alzheimer's model. *Science* **341**, 1399–1404 (2013).
13. Kounnas, M. Z. et al. LDL receptor-related protein, a multifunctional ApoE receptor, binds secreted beta-amyloid precursor protein and mediates its degradation. *Cell* **82**, 331–340 (1995).
14. Roberts, K. F. et al. Amyloid-beta efflux from the central nervous system into the plasma. *Ann. Neurol.* **76**, 837–844 (2014).
15. Iliff, J. J. et al. A paravascular pathway facilitates CSF flow through the brain parenchyma and the clearance of interstitial solutes, including amyloid beta. *Sci. Transl. Med.* **4**, 147ra111 (2012).
16. Biere, A. L. et al. Amyloid beta-peptide is transported on lipoproteins and albumin in human plasma. *J. Biol. Chem.* **271**, 32916–32922 (1996).
17. Mehta, P. D., Pirttila, T., Patrick, B. A., Barshatzky, M. & Mehta, S. P. Amyloid beta protein 1-40 and 1-42 levels in matched cerebrospinal fluid and plasma from patients with Alzheimer disease. *Neurosci. Lett.* **304**, 102–106 (2001).
18. Toledo, J. et al. Factors affecting Aβ plasma levels and their utility as biomarkers in ADNI. *Acta Neuropathol.* **122**, 401–413 (2011).
19. Rembach, A. et al. Changes in plasma amyloid beta in a longitudinal study of aging and Alzheimer's disease. *Alzheimer's Dement.* **10**, 53–61 (2014).
20. Nakamura, A. et al. High performance plasma amyloid-beta biomarkers for Alzheimer's disease. *Nature* **554**, 249–254 (2018).
21. Kuo, Y. M. et al. Amyloid-beta peptides interact with plasma proteins and erythrocytes: implications for their quantitation in plasma. *Biochem. Biophys. Res. Commun.* **268**, 750–756 (2000).
22. Rogers, J. et al. Peripheral clearance of amyloid beta peptide by complement C3-dependent adherence to erythrocytes. *Neurobiol. Aging* **27**, 1733–1739 (2006).
23. Gu, B. J. et al. P2X7 receptor-mediated scavenger activity of mononuclear phagocytes toward non-opsonized particles and apoptotic cells is inhibited by serum glycoproteins but remains active in cerebrospinal fluid. *J. Biol. Chem.* **287**, 17318–17330 (2012).
24. Yan P, et al. Peripheral monocyte-derived cells counter amyloid plaque pathogenesis in a mouse model of Alzheimer's disease. *J. Clin. Invest.* **132**, <https://doi.org/10.1172/JCI152565> (2022).
25. Munoz-Castro, C. et al. Monocyte-derived cells invade brain parenchyma and amyloid plaques in human Alzheimer's disease hippocampus. *Acta Neuropathol. Commun.* **11**, 31 (2023).
26. Baruch, K. et al. PD-1 immune checkpoint blockade reduces pathology and improves memory in mouse models of Alzheimer's disease. *Nat. Med.* **22**, 135–137 (2016).
27. Smyth, L. C. D. et al. Identification of direct connections between the dura and the brain. *Nature* **627**, 165–173 (2024).
28. Murdock, M. H. et al. Multisensory gamma stimulation promotes glymphatic clearance of amyloid. *Nature* **627**, 149–156 (2024).
29. Jiang-Xie, L. F. et al. Neuronal dynamics direct cerebrospinal fluid perfusion and brain clearance. *Nature* **627**, 157–164 (2024).
30. Tosto, G. & Reitz, C. Genome-wide association studies in Alzheimer's disease: a review. *Curr. Neurol. Neurosci. Rep.* **13**, 381 (2013).
31. Gandy, S. & Heppner, F. L. Microglia as dynamic and essential components of the amyloid hypothesis. *Neuron* **78**, 575–577 (2013).
32. Huang, X. et al. Leukocyte surface biomarkers implicate deficits of innate immunity in sporadic Alzheimer's disease. *Alzheimer's & dementia: the journal of the Alzheimer's Association* **19**, 2084–2094 (2023).
33. Jonsson, T. et al. Variant of TREM2 associated with the risk of Alzheimer's disease. *N. Engl. J. Med.* **368**, 107–116 (2013).
34. Chatterjee, P. et al. Plasma Aβ42/40 ratio, p-tau181, GFAP, and NfL across the Alzheimer's disease continuum: A cross-sectional and longitudinal study in the AIBL cohort. *Alzheimer's Dement.* **19**, 1117–1134 (2023).
35. Ellis, K. A. et al. The Australian Imaging, Biomarkers and Lifestyle (AIBL) study of aging: methodology and baseline characteristics of 1112 individuals recruited for a longitudinal study of Alzheimer's disease. *Int. Psychogeriatr.* **21**, 672–687 (2009).
36. Petersen, R. C. et al. Mild cognitive impairment: clinical characterization and outcome. *Arch. Neurol.* **56**, 303–308 (1999).
37. Winblad, B. et al. Mild cognitive impairment—beyond controversies, towards a consensus: report of the International Working Group on Mild Cognitive Impairment. *J. Intern. Med.* **256**, 240–246 (2004).
38. McKhann, G. et al. Clinical diagnosis of Alzheimer's disease: report of the NINCDS-ADRDA Work Group under the auspices of Department of Health and Human Services Task Force on Alzheimer's Disease. *Neurology* **34**, 939–944 (1984).



39. Rowe, C. C. et al. Amyloid imaging results from the Australian Imaging, Biomarkers and Lifestyle (AIBL) study of aging. *Neurobiol. Aging* **31**, 1275–1283 (2010).
40. Bourgeat, P. et al. Comparison of MR-less PiB SUVR quantification methods. *Neurobiol. Aging* **36**, S159–166 (2015).
41. Klunk, W. E. et al. The Centiloid Project: standardizing quantitative amyloid plaque estimation by PET. *Alzheimer's Dement.* **11**, 1–15 e11–14 (2015).
42. Bourgeat, P. et al. Implementing the centiloid transformation for (11)C-PiB and beta-amyloid (18)F-PET tracers using CapAIBL. *Neuroimage* **183**, 387–393 (2018).
43. Harrington, K. D. et al. The association of Abeta amyloid and composite cognitive measures in healthy older adults and MCI. *Int. Psychogeriatr.* **25**, 1667–1677 (2013).
44. Lim, Y. Y. et al. Effect of amyloid on memory and non-memory decline from preclinical to clinical Alzheimer's disease. *Brain* **137**, 221–231 (2014).
45. Lim, Y. Y. et al. Sensitivity of composite scores to amyloid burden in preclinical Alzheimer's disease: Introducing the Z-scores of Attention, Verbal fluency, and Episodic memory for Nondemented older adults composite score. *Alzheimer's Dement.* **2**, 19–26 (2016).
46. Donohue, M. C. et al. The preclinical Alzheimer cognitive composite: measuring amyloid-related decline. *JAMA Neurol.* **71**, 961–970 (2014).

## Acknowledgements

We thank Dr. Verena Wimmer and Dr. Carolina Chavez for their help with confocal microscopy. This work was supported by National Health and Medical Research Council (NHMRC) Project Grants - 2016803 to (Masters); ARC Future Fellowship FT120100581 (to Gu), NHMRC Project Grants - 1048082, 1061419, 1120095, and 110178 (to Gu), and State Government of Victoria (Victorian Government) - Operational Infrastructure Support Grant to the Florey Institute.

## Author contributions

X.H.: data collection, analysis, writing; C.F., Y. Li, Q.L., J.S., K.P., C. Dubois, C. Drysdale, R.R.: sample and data collection; J.D.: analysis. Y.Y.L., P.M.: cognitive tests; C.R.: brain imaging; Q.L., Y.P., L.J., H.C., R.M., P.M., Y.Y.L., A.B., Y. Lin, K.B.: results interpretation and writing; Y. Li: proofreading; C.M. and B.G.: design and writing.

## Competing interests

The authors declare no competing interests.

## Additional information

**Supplementary information** The online version contains supplementary material available at <https://doi.org/10.1038/s41467-024-52396-1>.

**Correspondence** and requests for materials should be addressed to Colin L. Masters or Ben J. Gu.

**Peer review information** *Nature Communications* thanks Serge Rivest, Charlotte Teunissen, and the other anonymous reviewer(s) for their contribution to the peer review of this work. A peer review file is available.

**Reprints and permissions information** is available at <http://www.nature.com/reprints>

**Publisher's note** Springer Nature remains neutral with regard to jurisdictional claims in published maps and institutional affiliations.

**Open Access** This article is licensed under a Creative Commons Attribution-NonCommercial-NoDerivatives 4.0 International License, which permits any non-commercial use, sharing, distribution and reproduction in any medium or format, as long as you give appropriate credit to the original author(s) and the source, provide a link to the Creative Commons licence, and indicate if you modified the licensed material. You do not have permission under this licence to share adapted material derived from this article or parts of it. The images or other third party material in this article are included in the article's Creative Commons licence, unless indicated otherwise in a credit line to the material. If material is not included in the article's Creative Commons licence and your intended use is not permitted by statutory regulation or exceeds the permitted use, you will need to obtain permission directly from the copyright holder. To view a copy of this licence, visit <http://creativecommons.org/licenses/by-nc-nd/4.0/>.

© The Author(s) 2024